Modeling demographic-driven vegetation dynamics and ecosystem biogeochemical cycling in NASA GISS's Earth system model (ModelE-BiomeE v.1.0)

Ensheng Weng[1,2], Igor Aleinov[1,2], Ram Singh[1,2], Michael J. Puma[1,2], Sonali S. McDermid[3], Nancy Y. Kiang[2], Maxwell Kelley[2], Kevin Wilcox[4], Ray Dybzinski[5], Caroline E. Farrior[6], Stephen W. Pacala[7], Benjamin I. Cook[2]

[1]Center for Climate Systems Research, Columbia University, New York, NY 10025, USA

[2]NASA Goddard Institute for Space Studies, 2880 Broadway, New York, NY 10025, USA

[3]Department of Environmental Studies, New York University, New York, NY 10003, USA

[4]Department of Ecosystem Science and Management, University of Wyoming, Laramie, WY 82071, USA

[5]Institute of Environmental Sustainability, Loyola University Chicago, Chicago, IL 60660, USA

[6]Department of Integrative Biology, University of Texas at Austin, Austin, TX 78712, USA

[7]Department of Ecology & Evolutionary Biology, Princeton University, Princeton, NJ 08544, USA

Corresponding author: Ensheng Weng (wengensheng@gmail.com; phone: 212-678-5585)

Submitted to **Geoscientific Model Development**

Abstract: We developed a new demographic vegetation model, BiomeE, to improve the representation of vegetation demographic dynamics and ecosystem biogeochemical cycles in the NASA Goddard Institute of Space Studies' ModelE Earth system model. This model includes the processes of plant growth, mortality, reproduction, vegetation structural dynamics, and soil carbon and nitrogen storage and transformations. The model combines the plant physiological processes of ModelE's original vegetation model, Ent, with minor adaptations to fit the new allometry and vegetation structure with the plant demographic and ecosystem nitrogen processes represented from Geophysical Fluid Dynamics Laboratory's LM3-PPA. For global applications, we added a new set of plant functional types to represent global vegetation functional diversity, including trees, shrubs, and grasses, and a new phenology model to deal with seasonal changes in temperature and soil water availability. Competition for light and soil resources is individual based, which makes the modeling of transient compositional changes and vegetation succession possible. BiomeE will allow ModelE to simulate long-term biogeophysical and biogeochemical feedbacks between the climate system and land ecosystems. BiomeE simulates, with fidelity comparable to other models, the dynamics of vegetation and soil biogeochemistry, including leaf area index, vegetation structure (e.g., height, tree density, size distribution, crown organization), and ecosystem carbon and nitrogen storage and fluxes. Further, BiomeE also allows for the simulations of transient vegetation dynamics and eco-evolutionary optimal community assemblage in response to past and future climate changes by incorporating core ecological processes, including demography, competition, and community assembly.

Key words: Biogeochemical cycles, Eco-evolutionary optimality, Ecosystem modeling, Plant traits, Vegetation dynamics

1 Introduction

Terrestrial ecosystems play a critical role in the climate system by regulating exchanges of energy, moisture, and carbon dioxide between the land surface and the atmosphere (Sellers, 1997; Pielke et al., 1998; Meir et al., 2006). In turn, climate change has significantly affected vegetation photosynthesis, water use efficiency, mortality, regeneration, and structure through gradual changes in temperature and atmospheric CO_2 concentration ($[CO_2]$) together with shifts in climate extremes (Brando et al., 2019; McDowell et al., 2020; Keenan et al., 2013; Huang et al., 2015). These responses have triggered vegetation structural and compositional shifts. For example, global forest mortality has increased in recent years (Allen et al., 2010; Anderegg et al., 2012), tree sizes have decreased (Zhou et al., 2014; McDowell et al., 2020), and species composition has shifted to more opportunistic species (Clark et al., 2016; Brodribb et al., 2020). The shifts in vegetation function, composition, and structure can change the boundary conditions of the land surface and affect the climate system (Nobre et al., 1991; Avissar and Werth, 2005; Garcia et al., 2016; Green et al., 2017; Zeng et al., 2017). Realistic simulation of these processes is therefore critical for Earth system models (ESMs).

The vegetation dynamics in ESMs are usually simulated using dynamic global vegetation models (DGVMs) (Prentice et al., 2007), most of which are simplified in their representation of ecological processes. The core assumptions of many vegetation models are a big-leaf canopy, vegetation represented by only a few plant functional types (PFTs), single cohort-based vegetation dynamics ("single-cohort" assumption, where the vegetation community at a land unit are simulated as a collection of identical plants), lumped-pool-based biogeochemical cycles and first order decay of soil organic matter. The competition of plant individuals and vegetation types is approximately simulated as a function of productivity or Lotka-Volterra equations to predict

fractional PFT coverage (e.g., SDVGM, HYBRID, TRIFFID) (Friend et al., 1997; Woodward et al., 1998; Sitch et al., 2003). These simplifying assumptions make it possible to simulate the complex interactions of biological and ecological processes at the global scale.

These models are generally successful in reproducing land surface carbon, energy, and water fluxes after extensive tuning against data from sites, observational networks, and satellite remote sensing. However, the uncertainty of model predictions is high, and predictions can diverge substantially across different models (Friedlingstein et al., 2014; Arora et al., 2020). Lack of functional diversity and community assembly processes is one of the key issues in the vegetation modeling of ESMs, which makes the models unable to predict transient dynamics of vegetation composition and structure. A more mechanistic design that uses the fundamental principles of ecology to simulate the emergent properties of ecosystems for predicting ecosystem dynamics may therefore be necessary (Weng et al., 2017; Scheiter et al., 2013).

To this end, extensive efforts have been made to improve the representation of transient vegetation dynamics based on ecological theories and conceptual models. Two pivotal advances have been made in ecological vegetation modeling: 1) Demographic processes and trait-based representation of processes have been developed to improve the representation of functional diversity and size (Fisher et al., 2015; Weng et al., 2015; Pavlick et al., 2013; Argles et al., 2020) and 2) eco-evolutionary optimal and game theoretical approaches have been proposed to predict the flexibility of parameters and processes (McNickle et al., 2016; Weng et al., 2017). These concepts are mainly applied in modeling photosynthesis (Wang et al., 2017; Prentice et al., 2014), allocation (Farrior et al., 2013; Dybzinski et al., 2015), and evolutionarily stable strategy of plant traits (Falster et al., 2017; Weng et al., 2017). These ideas for incorporating ecological

and evolutionary principles into ESMs have been summarized in several recent review papers (Harrison et al., 2021; Franklin et al., 2020; Kyker-Snowman et al., 2022).

There are still major challenges to integrating these more sophisticated ecological modeling approaches into the complex land models of ESMs, where the explicit simulations of energy, water, and carbon fluxes at high frequencies are required for interacting with the atmosphere and climate system. The details of vegetation dynamics, including the key functions from leaf photosynthesis, respiration, biogeochemical fluxes between pools, demographic processes, community assembly, vegetation structure, and competition output, must be well-organized hierarchically and computed efficiently (Fisher and Koven, 2020; Franklin et al., 2020). Representing these processes in ESMs, however, can complicate model structure and behavior, especially for the interaction between physiology and vegetation composition, and cause large increases in the computational burden. Thus, the implementation of detailed vegetation demographic processes and size categories into ESMs would benefit from more parsimonious approaches.

Including highly complex processes does not necessarily increase model predictive skills (Famiglietti et al., 2021; Forster, 2017; Hourdin et al., 2017). On the contrary, it may greatly obscure model transparency and increase uncertainty, and positive feedbacks in these processes may result in large and unanticipated shifts of vegetation states. Any small differences in model setting or even parameter differences can result in distinct predictions, especially in vegetation structure, which is supposed to be predicted by these types of models. These processes make demographic vegetation models often unreliable when compared to the well-tuned "single-cohort" vegetation models that simplify the reproduction and mortality as growth and turnover of continuous biomass pools. Additionally, the long history of land models and the requirements of

113 backward compatibility (i.e., reversing the model to its previous functions) mean developers
114 must often build their new functions on top of previous modeling assumptions and coding
115 structure (Fisher and Koven, 2020), adding up to multiple adjustments of previous processes and
116 making the model untraceable.

117 To explicitly model the transient dynamics of ecosystems in ESMs while preserving model
118 traceability, we need clear assumptions, detailed physical processes, and traceable model
119 structure. For the best chance of accurate predictions outside of the model's testing data, model
120 processes should be based on the fundamental biological and ecological principles to predict
121 ecosystem emergent properties, instead of fitting the emergent patterns directly as many models
122 do currently. To achieve this, we need to properly represent the tradeoffs of plant traits, balance
123 the complexity of the model structure and priority for the processes that are required by the
124 general circulation model (GCM), and also make model assumptions transparent and processes
125 robust. These requirements make it difficult to fully implement the modeling approaches that are
126 well-developed in the ecological modeling community.

127 This paper describes a vegetation demographic and soil organic decomposition model that
128 is incorporated into the NASA Goddard Institute for Space Studies (GISS) Earth system model,
129 ModelE (Kelley et al., 2020). Our goal is to develop a parsimonious and transparent terrestrial
130 ecosystem model that 1) allows ModelE to simulate the ecological dynamics of terrestrial
131 ecosystems and vegetation at the global scale and 2) sets up a modeling framework for solving
132 some of the major challenges for incorporating important ecological mechanisms into ESMs. For
133 (1), we have incorporated core ecosystem processes, including plant growth, demography,
134 community assembly, and ecosystem carbon and nitrogen cycles. For (2), we have developed
135 PFTs that are plant trait-based and a competition scheme that is individual-based. In this paper,

we describe this model in detail, and evaluate its performance compared to both observations and other state-of-the-art DGVMs.

2 Model Description

2.1 GISS ModelE and BiomeE overview

ModelE has a land model for representing land surface hydrology (TerraE) (Rosenzweig and Abramopoulos, 1997; Schmidt et al., 2014) and a vegetation biophysics scheme (from the Ent Terrestrial Biosphere Model; TBM) (Ito *et al.* 2020; Kelley *et al.* 2020; Schmidt *et al.* 2014), with fixed vegetation traits (e.g., leaf mass per area, C:N ratio), fixed biomass, canopy height, and plant density, and seasonal leaf area index prescribed from a satellite-derived data set (Ito et al., 2020). The Ent TBM calculates canopy radiative transfer (Friend & Kiang 2005), canopy albedo, canopy conductance, photosynthesis, autotrophic respiration, and some phenological behaviors of leaf biophysics (Kim et al., 2015). The carbon allocation scheme of Kim et al. (2015) is used in ModelE with prescribed canopy structure and LAI, routing the carbon that would otherwise be allocated to plant tissues via growth instead directly as litter into soil carbon pools, thus conserving carbon for fully coupled carbon cycle simulations, but resulting possibly in imbalanced plant carbon reserve pools where the prescribed canopy structure is not in equilibrium with the simulated climate (Ito et al., 2020).

The Biome Ecological strategy simulator (BiomeE) is derived from Geophysical Fluid Dynamics Laboratory's vegetation model, LM3-PPA (Weng et al., 2019, 2015, 2017). It simulates plant physiology, vegetation demography, adaptive dynamics (eco-evolutionary adaptation), and ecosystem carbon, nitrogen, and water cycles (Fig. 1). In this model, the PFTs are defined by a set of combined plant traits with their values sampled from the observed ranges to represent a

specific plant type. Individual plants are categorized into cohorts and arranged in different vertical canopy layers according to their height and crown area following the rules of the Perfect Plasticity Approximation model (PPA, Strigul et al., 2008). Sunlight is partitioned into canopy crown layers according to Beer's law. The cohort is the basic unit to carry out physiological and demographic activities, e.g., photosynthesis, respiration, growth, reproduction, mortality, and competition with other individuals.

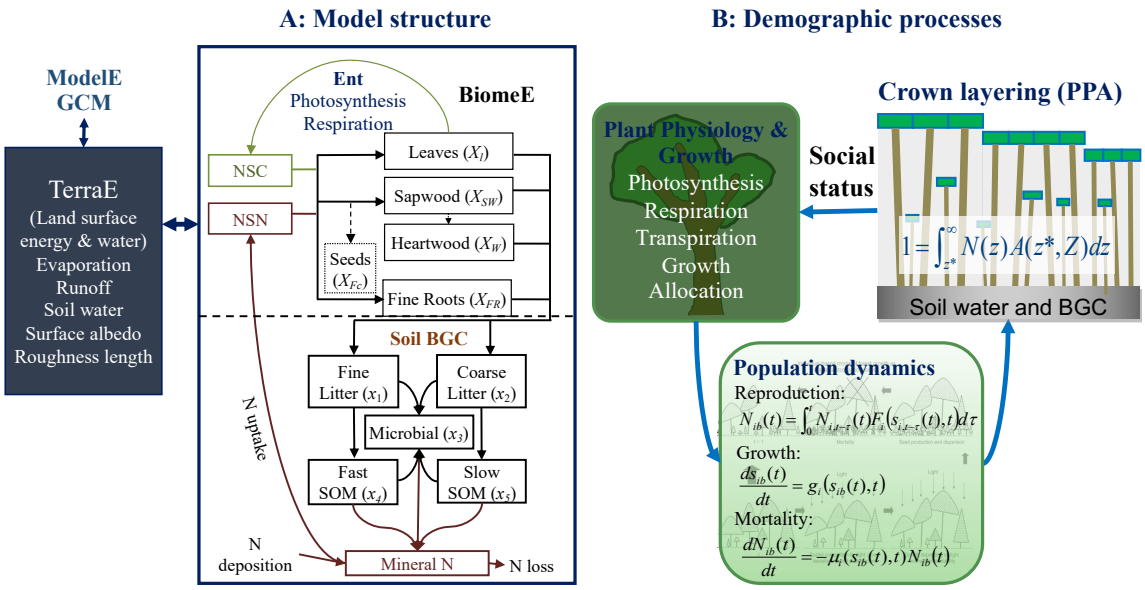

Figure 1 Schematic diagram of the coupling of BiomeE into ModelE

Panel A shows the structure of carbon and nitrogen pools and fluxes, and the interactions of BiomeE with TerraE, the land surface model in ModelE. The lines are the flows of carbon (green), nitrogen (brown), and coupled carbon and nitrogen (black). The green box is for carbon only. The brown boxes are N pools. The black boxes are for both carbon and nitrogen pools. The C:N ratios of leaves, wood, fine roots, and microbes are fixed and those of liters and SOM pools are dynamic with input and output. Panel b shows the demographic processes of BiomeE and the key processes of population dynamics.

The demographic processes generate and remove cohorts and change the size and density of plant individuals in the cohorts. With explicit description of cohort size, organization, and

composition during a model run, the model simulates competition for light and soil resources, community assembly and vegetation structural dynamics. These processes are hierarchically organized in this model and run at various time steps: half-hourly or hourly for plant physiology and soil organic matter decomposition, daily for growth and phenology, and yearly for demography.

We coupled the standalone BiomeE into ModelE's land model for simulating global dynamics of vegetation and biogeochemical cycles and their feedback to the climate system . For extending this model to the global scale, we designed a new set of PFTs to represent the functional diversity of global vegetation and a new phenological scheme to deal with temperature and water seasonality. Leaf photosynthesis processes are taken from ModelE's existing vegetation model, Ent (Kim et al., 2015), and used to calculate the carbon budget that drives vegetation dynamics. Plant growth and demographic processes and the soil organic matter decomposition and nitrogen cycle processes are from BiomeE (Fig. 1). The land surface energy and water fluxes are calculated by TerraE with land surface characteristics jointly defined by the vegetation model.

Plant functional types

In this model, we use a set of continuous plant traits to define plant functional types, so that we can simulate plant emergent properties (such as dominant plant types, vegetation compositional changes, etc.) in response to climate changes based on the underlying plant physiological properties and ecological principles through eco-evolutionary modeling in the future. For example, life forms are defined by the continuums characterized by wood density (woody vs. herbaceous), height growth coefficient (tree vs. shrub), and leaf mass per unit area (LMA, for evergreen vs. deciduous). Deciduousness is defined by cold resistance (evergreen vs. cold

deciduous), and drought resistance (evergreen vs. drought deciduous). Grasses are simulated as tree seedlings with all stems senescent along with leaves at the end of a growing season. The individuals are reset back to initial size each year and the population density is also reset using the total biomass of current cohort and predefined initial size of grasses. The photosynthesis pathway is predefined as C_3 or C_4.

We defined 9 PFTs for our test runs in this paper to roughly represent global vegetation functional diversity (Table 1) according to their life form (tree, shrub, and grass), photosynthesis (C_3 and C_4), and leaf phenology (evergreen and deciduous).

Table 1 Plant functional types used in BiomeE

Plant functional types	V_{cmax}	LMA (kg C m^{-2})	ρ_W (kg C m^{-3})	α_Z	$T_{0,c}$	$\beta_{0,D}$	PS pathway
1. Tropical evergreen broadleaf	18	0.07	360	30	15	0	C_3
2. Temperate/boreal evergreen needleleaf	18	0.14	300	30	-80	0	C_3
3. Temperate/boreal deciduous broadleaf	22	0.025	350	30	15	0	C_3
4. Tropical drought deciduous broadleaf	20	0.03	250	30	15	0.2	C_3
5. Boreal deciduous needleleaf	20	0.03	300	30	15	0.0	C_3
6. Cold shrub	18	0.025	360	20	15	0.1	C_3
7. Arid shrub	18	0.03	360	20	15	0.1	C_3
8. C3 grass	20	0.025	90*	10	5	0.2	C_3
9. C4 grass	15	0.025	90*	10	5	0.2	C_4

LMA: leaf mass per unit area, ρ_W: wood density, α_Z: Height coefficient, $T_{0,c}$: Critical temperature for phenology offset, $\beta_{0,D}$: critical soil moisture index for the offset of phenology, PS: photosynthesis pathway, E: evergreen, C: cold-deciduous, D: drought-deciduous. *Grass stem density is calculated as tissue biomass divided by stem volume. The tissue density of grass's stems is as high as wood.

All PFTs go through the same set of plant physiological and demographical processes in the model and derive different emergent properties due to the differences in parameters, rather than differences in processes (except C_3 and C_4). With these different strategies, they have their advantages and risks in different environments. An advantage of this continuous parameter design is that one PFT can switch to another by changing its parameters (except C_3 and C_4 photosynthesis pathways). This opens the way for eco-evolutionary and ecological community assembly simulation to explore the competitively optimal plant traits as environments change.

Phenology

Phenology types are defined by two parameters, a critical low temperature and a critical soil moisture index, that are used to trigger leaf fall. These two parameters define 4 phenological types with their possible factorial combinations: evergreen, drought-deciduous, cold-deciduous, and drought-cold-deciduous. Evergreen PFTs have high resistances to cold (i.e., very low critical temperature) and drought (very low soil drought). Cold and drought deciduous PFTs have low critical temperature and soil drought index, respectively. These phenological types represent different strategies of dealing with environmental stresses and pressure of competition. It is possible that the evergreen would be more competitive in high seasonality regions (e.g., evergreen in boreal regions), though the first response of plants to harsh environments (e.g., cold or dry) is to shed their leaves. Our definition of phenology is designed to make it possible to evaluate the competitively optimal strategy in future studies.

For the cold-deciduous PFTs (3 and 5), we used the growing degree days above 5 °C (GDD_5) to control the timing of phenological onset and a critical low temperature (T_m) to control the offset. GDD_5 is calculated from the days that temperature starts to increase from the coldest days in the non-growing season. The critical value of GDD that the plants require for growth

(GDD_c) is defined as a function of chilling days in the non-growing season (Prentice et al., 1992):

$$GDD_c = a_0 + d \cdot e^{-b \cdot N_{CD}}, \quad (1)$$

where, N_{CD} is the days of the cold period in nongrowing season before bud burst, a_0 is the minimum GDD_c (50) when the cold period is sufficiently long, d is the maximum addition of GDD_c (800) when there is no cold period (i.e., N_{CD}=0), b is a shape coefficient (0.025). These parameters are tunable and should change with acclimate to new climates.

The running mean temperature that represents the mean temperatures over a short period of time is calculated as:

$$\begin{cases} T_m(i) = T_d(i), & when\ i = 1 \\ T_m(i) = 0.8T_m(i-1) + 0.2T_d(i), & when\ i \geq 2 \end{cases}, \quad (2)$$

We used an index of cold condition (accumulative low temperature, ALT) to make sure the low temperature signal is persistent and differentiates the signal of the seasonal temperature changes and the stochastic low temperature stresses in growing seasons. The critical temperature for triggering leaf senescence (T_c) is calculated as a function of the number of growing days (N_{GD}).

$$T_c = T_{0,c} - s \cdot e^{-c \cdot (\max(0, N_{GD} - L0))}, \quad (3)$$

where, $T_{0,c}$ is the highest critical temperature when N_{GD} is sufficiently long, s is the range that a critical temperature can change, c is a shape parameter, *L0* defines the lowest critical temperature ($T_{0,c}$ -s) when N_{GD} is smaller than *L0*. The rationale in this equation is that when a growing period is not long enough, plants need a lower T_c to trigger leaf fall so that they can have a growing season that is not too short. This setting is based on the thermal adaptation analysis of Yuan *et al.* (2011).

For the drought deciduous PFTs (tropical drought deciduous broadleaf, arid shrub, C_4 grass), we used a soil moisture index (s_D) to start and end a growing season.

$$s_D = \sum_{i=1}^{n} Min\left(1.0, max\left(\frac{\theta_i - \theta_{WP,i}}{\theta_{HC,i} - \theta_{WP,i}}, 0.0\right)\right), \quad (4)$$

where i is the soil layer in root zone, θ is soil water content (vol./vol.), θ_{WP} is wilting point, and θ_{HC} is soil water holding capacity. The critical soil moisture values that trigger new leaf growth and leaf fall are defined as PFT-specific parameters. We slightly tuned these two parameters according to the soil moistures where the deciduous PFTs' leaves start to grow or fall. Usually, the critical soil moisture for starting new leaf growth is higher than the soil moisture levels that trigger leaf fall so that the plants can have a stable growing season.

Plant demography and biogeochemical cycles

Allometry and Plant architecture

The plant allometry and architecture are critical for plant resources allocation, light capture, and soil water and nutrients uptake. The allometry equations are the same as those used in LM3-PPA (Weng et al., 2015; Farrior et al., 2013):

$$\begin{cases} A_C = \alpha_C D^{\theta_C} \\ Z = \alpha_Z D^{\theta_Z} \\ S = 0.25\pi\rho\Lambda\alpha_H D^{2+\theta_H} \\ A_L^* = l_{max} A_C \\ A_{FR}^* = \varphi_{RL} l_{max} A_C \end{cases}, \quad (5)$$

where D is tree diameter; A_C is crown area; Z is plant height; S is woody biomass (sapwood plus heartwood); α_C and α_Z, are the scaling factors for crown area and plant height, respectively; θ_C and θ_Z are the exponents for crown area and tree height, respectively; π is ratio of a circle's circumference to its diameter; ρ is wood density (kg C m^{-3}); Λ is the taper factor from a cylinder

to a tree with the same D; A_L^* and A_{FR}^* are the target surface area of leaves and fine roots, respectively; φ_{RL} is the area ratio of leaves to roots. l_{max} is the maximum leaf area per unit crown area, defined as a function of plant height (Z):

$$l_{max}(Z) = L_{max,0}(Z + h_0)/(Z + H_0), \quad (6)$$

where $L_{max,0}$ is the maximum crown LAI when a tree is sufficiently tall, Z is tree height, h_0 is a small number that makes a minimum l_{max} ($L_{max,0}$ (h_0/H_0)) when tree height is close to zero, and H_0 is a curvature parameter.

Plant growth and allocation of carbon and nitrogen to plant tissues

The allocation of NPP wood, leaves, and roots is affected by climate and forest age (Xia et al., 2019; Litton et al., 2007). However, vegetation models cannot capture these patterns well at large spatial scales, even if the adaptive responses to climate and forest ages are considered (Xia et al., 2019, 2017), partly because of the absence of explicit representation of shifts in species composition and competition between individuals (Dybzinski et al., 2015; Franklin et al., 2012). BiomeE has an optimal growth scheme that drives the allocation of carbon and nitrogen to leaves, fine roots, and stems based on the optimal use of resources and light competition (Weng et al., 2019). In this scheme, the growth of new leaves and fine roots follows the growth of woody biomass (i.e., stems), and the area ratio of fine roots to leaves is kept constant during the growing season. The allocation of available carbon between structural (e.g., stems) and functional (e.g., leaves and fine roots) tissues is optimal for light competition at given nitrogen availability.

Mathematically, differentiating the stem biomass allometry in Eq. 5 with respect to time, using the fact that *dS/dt* equals the carbon allocated for wood growth (G_W), gives the diameter growth equation:

$$\frac{dD}{dt} = \frac{G_W}{0.25\pi\Lambda\rho_w\alpha_z(2+\theta_z)D^{1+\theta_Z}} \quad (7)$$

This equation transforms the carbon gain from photosynthesis to the diameter growth that results from wood allocation and allometry (Eq 5). With an updated tree diameter, we can calculate the new tree height and crown area using allometry equations, and the targets of leaf and fine root biomass (Eq. 5). Generally, the growing-season average allocations of carbon and nitrogen to different tissues are governed by two parameters: the maximum leaf area per unit crown area (l_{max}) and fine root area per unit leaf area (φ_{RL}) (Eq. 5). The optimal-growth allocation scheme combined with explicit competition for light and soil resources in our model makes it possible to simulate the underlying processes that determine emergent allocation patterns (Weng et al., 2019; Farrior et al., 2013; Dybzinski et al., 2011; Farrior, 2019).

Reproduction and Mortality

At a yearly time-step, the cumulative carbon and nitrogen allocated for reproduction by a canopy cohort over the growing season length, *T,* is converted to seedlings according to the initial plant biomass (S_0) and germination and establishment probabilities (p_g and p_e, respectively). Generally, the population dynamics can be described by a variant of the von Foerster equation (von Foerster, 1959):

$$N(S_0,t) = \frac{p_g p_e}{S_0}\int_0^T N(\tau)G_F(\tau)d\tau$$
$$\frac{dN(s,t)}{dt} = -\mu(s,t)N(s,t). \quad (8)$$

where $N(S_0, t)$ is the spatial density of newly generated seedlings, $N(\tau)$ is the spatial density of this cohort of trees at time τ, G_F is the carbon allocation to seeds, and μ is PFT-specific mortality parameter

Each PFT has a canopy-layer-specific background mortality rate that is assigned from the literature. These background rates are assumed to be size-independent for the canopy layer trees, but size-dependent for understory trees. Many factors affect tree mortality, such as light, size, competition crown damage, hydraulic failure, trunk damage etc. (Zuleta et al., 2022; Lu et al., 2021). These factors result in high mortality rates of seedlings and old trees (i.e., a "U-shaped" mortality curve). We use the following equation to delineate a mortality rate that varies with social status (crown layers), shade effects, and tree sizes:

$$\mu(s,t) = \mu_0(1 + f_L f_s) f_D \quad (9)$$

where f_L is the shade effects on mortality ($f_L = \sqrt{L-1}$), f_S is seedling mortality when a tree is small ($f_s = A_{SD} e^{-B_{SD} \cdot D}$), and f_D represents the size effects on the mortality of adult trees ($f_D = m_s \frac{e^{A_D(D-D_0)}}{1+e^{A_D(D-D_0)}}$). L is the layer this plant is in (L=1 for the canopy layer and 2 for the second, and so on), A_{SD} is the maximum multiplier of mortality rate for the seedlings in the understory layers, B_{SD} is the rate of mortality decreasing as tree diameter (D) increases, m_s is the maximum multiplier of mortality rate for large-sized trees, D_0 is the diameter at which the mortality rate increases by m_s /2, and A_D is a shape parameter (i.e., the sensitivity to tree diameter).

Crown self-organization and layering

Tree crowns are arranged into different vertical canopy layers according to tree height and crown area if their total crown area is greater than the land area following the rules of the PPA model (Strigul et al., 2008). In PPA, individual tree height is defined as the height at the top of

the crown, and all leaves of a given cohort are assumed to belong to a single canopy layer. The height of canopy closure for the top layer is referred to as critical height (Z^*, the height of the shortest tree in the layer) and is defined implicitly by the following equation:

$$k(1-\eta) = \sum_i \int_{Z^*}^{\infty} N_i(Z,t) A_{CR,i}(Z^*, Z) dZ \quad (10)$$

where $N_i(Z,t)$ is the density of PFT *i* trees of height *Z* per unit ground area; $A_{CR,i}(Z^*, Z)$ is the crown area of an individual PFT *i* tree of height *Z*; η is the proportion of each canopy layer that remains open on average due to wind and imperfect spacing between individual tree crowns, and *k* is the ground area. The top layer includes the tallest cohorts of trees whose collective crown area sums to $1-\eta$ times the ground area; lower layers are similarly defined.

All the trees taller than the critical height can get full sunlight and all trees below this height are shaded by the upper layer trees. Trees within the same layer do not shade each other, but there is self-shading among the leaves within individual crowns. Cohorts in a sub-canopy layer are shaded by the leaves of all taller canopy layers. In each canopy layer, all cohorts are assumed to have the same incident radiation on the top of their crowns. Note, the gap fraction η is necessary to allow additional light penetration through each canopy layer for the persistence of understory trees in monoculture forests in which the upper layer crowns build a physiologically-optimal number of leaf layers (Farrior et al., 2013). The grasses only form one layer. Those individuals who cannot stay in that layer because of limited space will be killed (i.e., when the total grass crown area is larger than the land area).

Ecosystem carbon and nitrogen biogeochemical cycles

Ecosystem biogeochemical cycles (carbon and nitrogen in this model) are driven by plant and microbial demographic processes. There are seven pools in each plant: leaves, fine roots,

sapwood, heartwood, fecundity (seeds), and non-structural carbohydrates and nitrogen (NSC and NSN, respectively). The carbon and nitrogen in plant pools enter soil pools with the mortality of individual trees and the turnover of leaves and fine roots. Soil has a mineral nitrogen pool for mineralized nitrogen and five soil organic matter (SOM) pools for carbon and nitrogen: metabolic litter (x_1), structural litter (x_2), microbial (x_3), and fast (x_4) and slow-turnover (x_5) SOM pools.

The microbial pool plays a central role in the transfer and decomposition of SOM. The decomposition processes are simulated by a model modified from Manzoni et al. (2010). The technical details have been described in Weng et al. (2019, 2017). The decomposition rate of a SOM pool is determined by the basal turnover rate together with soil temperature and moisture following the formulation of the CENTURY model (Parton et al., 1988, 1987). The microbial carbon use efficiency (transfer from litter to microbial matter) is a function of litter nitrogen content, following the model of Mazoni et al. (2010).

The N mineralization in decomposition is determined by microbial nitrogen demand, SOM's C:N ratio, and decomposition rate. In the high C:N ratio SOM, microbes must consume excess carbon to get enough nitrogen for growth. By contrast, in the low C:N ratio SOM, microbes must release excess nitrogen to get enough carbon for energy. Depending on the C:N ratios of SOM, soil microbes may be limited by either C or N.

The out-fluxes of C and N from the i^{th} pool (dC_i and dN_i, respectively) are calculated by:

$$\begin{aligned} dC_i &= \xi(T,M)\rho_i Q C_i, \\ dN_i &= \xi(T,M)\rho_i Q N_i \ , \end{aligned} \tag{11}$$

where ξ is the response function of decomposition to soil temperature (T) and moisture (M), ρ_i is the basal turnover rate of the i^{th} litter pool at reference temperature and moisture, QC_i is the C content in i^{th} pool, and QN_i is the N content in the i^{th} pool.

The new microbial growth (dM) is calculated as the co-limit of available carbon and nitrogen mobilized at this step:

$$dM_i = Min(\varepsilon_0 \cdot dC_i, \Lambda_{microbe} \cdot dN_i), \quad (12)$$

where ε_0 is default carbon-use efficiency of litter decomposition (0.4) and Λ_{microbe} is a microbe's C:N ratio, which is a fixed value (10 in this model). The soil heterotrophic respiration (R_h) is the microbial respiration (i.e., the difference between carbon consumption and new microbial growth), and the total N mineralization rate ($N_{\text{mineralized}}$) is calculated as the sum of mineralized N in the SOM pools and microbial turnover:

$$\begin{aligned} R_h &= \sum_{i=3}^{5} dC_i - \sum_{i=4}^{5} M_i, \\ N_{mineralized} &= \sum_{i=3}^{5} dN_i - \sum_{i=3}^{5} m_i/\Lambda_{\text{microbe}} \end{aligned} \quad (13)$$

The R_h releases to atmosphere as CO_2. Mineralized N enters the mineral N pool for plants to use. The dynamics of the mineral N pool is represented by the following equation:

$$\frac{dN_{mineral}}{dt} = N_{deposition} + N_{mineralized} - U - N_{loss}, \quad (14)$$

where $N_{\text{deposition}}$ is N deposition rate, assumed to be constant over the period of simulation; N_m is the N mineralization rate of the litter pools (fast and slow SOM and microbes); U is the N uptake rate (Kg N m^{-2} $hour^{-1}$) of plant roots; and N_{loss} includes the loss of mineralized N by denitrification and runoff. The N deposition ($N_{\text{deposition}}$) is the only N input to ecosystems, and we set nitrogen fixation as zero in this version of the model.

3 Model Test runs

For our comparison of model performance against observations and other models, we used the full demographic version of BiomeE (described above) and also designed a "single-cohort" version of the model to benchmark our demographic implementations. In the single-cohort model, the mortality of trees is simulated as the turnover of woody biomass, and the fecundity resources (carbon and nitrogen) are used to build the same-sized parent trees, instead of seedlings growing from understory layers. If the total crown area of the trees in this cohort is greater than the land area, the extra trees will be removed to make the total crown area less than or equal to the land area. At equilibrium, the turnover of woody biomass is equal to the new growth each year and the new trees generated from fecundity resources are killed by self-thinning. The single-cohort model uses the mean state of the canopy layer trees to represent the characteristics of the whole community. This single-cohort model performs like the traditional biogeochemical models and simplifies vegetation computation.

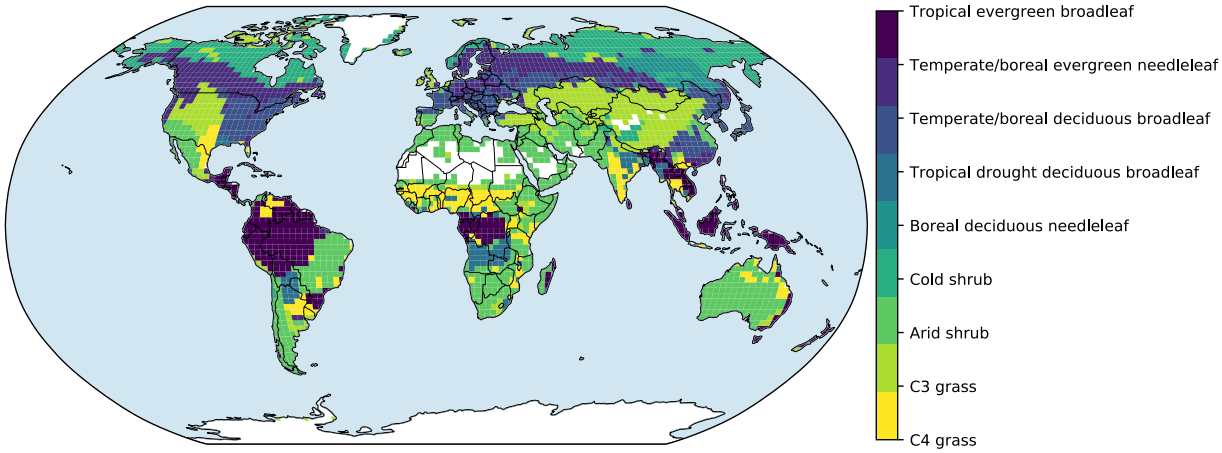

Figure 2. Prescribed global distribution of plant functional types. Data is from the Ent Global Vegetation Structure map.

In the test runs, the distribution of PFTs was from the Ent vegetation map (Ito et al., 2020), which is derived from 2004 MODIS land cover and PFT data products (Friedl et al., 2010) and climate data (Fig. 2). For these simulations, croplands and pastures were replaced by the potential natural vegetation types.

Forcing data are from the TRENDY project CRU-NCEP data (Sitch et al., 2015) and have a 6-hour time step at a spatial resolution of 0.5°x0.5°. These data are available at the website https://www.uea.ac.uk/web/groups-and-centres/climatic-research-unit/data.

We aggregated these data into 2.0°x2.5° grid cells and used thirty years' of data (1988~2017) to force the model to run for 600 years, which is long enough for the model to approach equilibrium states for both vegetation and soil carbon pools. These data include temperature, precipitation, shortwave radiation, longwave radiation, specific humidity, and wind speed (U and V directions). We interpolated the radiation data (R_S) into half-hour timesteps based on the sun zenith angle (θ_S) and radiation penetration rate calculated from data.

$$R_S(t) = \left(\frac{R_{H6}}{S^* coscos\ \theta_s(H6)}\right) S^*\ cos\ cos\ \theta_s(t)\ , \qquad (15)$$

where S^* is solar constant (1362 W/m^2). Other variables are linearly interpolated to the model time steps, which is half hourly in this study. CO_2 concentration is set at the model default level (350 ppm) in our model runs.

Data sources for model evaluation

Gross primary productivity (GPP) data are from a global retrieval of surface turbulent fluxes including latent heat, sensible heat, and GPP using remote sensing observations. These data are on a 1°×1° geographic grid at a monthly time step based on an Artificial Neural Network

retrieval algorithm (Alemohammad et al., 2017). This algorithm uses six remotely sensed observations as input: Solar Induced Fluorescence (SIF), Air Temperature, Precipitation, Net Radiation, Soil Moisture, and Snow Water Equivalent. The data are available from 2007 to 2015. **The tree height data** are from spaceborne light detection and ranging (lidar) global map of canopy height at 1-km spatial resolution developed by Simard et al. (2011). These authors used the 2005 data from the Geoscience Laser Altimeter System (GLAS) aboard ICESat (Ice, Cloud, and land Elevation Satellite) to derive global forest canopy heights. **Biomass data** are from a Global 1-degree Maps of Forest Area, Carbon Stocks, and Biomass, 1950-2010 developed by Hengeveld et al. (2015). **Soil carbon data** are from Food and Agriculture Organization (FAO) Harmonized World Soil Database (version 1.2), updated by Wieder et al. (2014).

MsTMIP model simulation data

We chose six model simulations (BiomeBGC, CTEM, CLM4, LPJ, Orchidee, VEGAS) from the Multi-scale Synthesis and Terrestrial Model Intercomparison Project (MsTMIP) (Huntzinger et al., 2013) to compare against our model simulations. These models are well-developed and widely used in Earth system models, representing the state-of-art of current land vegetation model development. MsTMIP provided prescribed land use types for all the participant models. However, it is up to the participant models for disturbance impacts on ecosystems (Huntzinger et al., 2013). MsTMIP conducted five sets of experimental runs with different climate forcing, land-use history, atmospheric CO_2 concentration, and nitrogen deposition. In this study, we used the SG1 simulation experiment because it is driven by the 1901~2010 climate forcing data with constant CO_2 concentration and constant land cover (Huntzinger et al., 2013), which are the closest to our model runs.

Selected Grid Cells for Comparison

To illustrate model behavior, we selected 8 grid cells that cover boreal forests, temperate forests, tropical forests, C_4 grasslands, and arid shrublands to show the simulated ecosystem development patterns across the climate zones with different dominant PFTs (Table 2). Brazil Tapajos (TPJ), Oak Ridge (OKR), Harvard Forest (HF), Manitoba old black spruce site (MNT), and Bonanza Creek (BNC) are covered by tree PFTs. Konza long-term ecological research station (LTER) (KZ) is C_4 grass. Walnut Gulch Kendall (WKG) and Sevilleta LTER (SV) are covered by arid shrubs. These sites were chosen because they have extensive data on vegetation and climate conditions for future comparisons.

Table 2 Sites for simulated ecosystem development illustration

Site	Dominant PFT	Coordination	Mean Temperature (°C)	Annual Precipitation (mm)
Bonanza Creek (BNC)	Broadleaf deciduous	63.92°, -145.38°	-3.1	269
Manitoba old black spruce site (MNT)	Evergreen needleleaf	55.88°, -98.48°	-3.2	520
Harvard Forest (HF)	Broadleaf deciduous	42.54°, -72.17°	8.5	1050
Oak Ridge (OKR)	Broadleaf deciduous	35.96°, -84.29°	13.7	1372
Konza LTER (KZ)	C_4 grass	39.08°, -96.56°	12.4	835
Sevilleta LTER (SV)	Arid shrub	34.36°, -106.88°	12.7	365
Walnut Gulch Kendall (WGK)	Arid shrub	31.74°, -109.94°	17.7	350
Brazil Tapajos (TPJ)	Broadleaf evergreen	-2.86°, -54.96°	26	1820

4 Results

4.1 Simulated vegetation structural and ecosystem carbon dynamics

In the forest sites, the simulated vegetation structure by the full demographic model changes with the growth, regeneration, and mortality processes (Fig. 3). It can be separated into three stages

according to the canopy crown dynamics: 1) open forest stage, 2) self-thinning stage, and 3) stabilizing stage. In the open forest stage, the crown area index (CAI) is less than 1.0 and all the individuals are in full sunlight. The tree crowns grow rapidly to occupy the open space (Fig. 3: a). In the self-thinning stage, the open space is filled by the crowns of similar sized trees (i.e., the forest is closed) and canopy trees are continuously pushed to the lower layer(s) (i.e., self-thinning) and the CAI continues to increase due to the limited space with growing tree crowns (i.e., the new spaces vacated from the canopy trees' mortality cannot meet the space demand from crown growth). The sizes of trees in the canopy layer are still similar in this period (Fig. 3: b and c) and the critical height (the height of the shortest tree in the canopy layer) keeps increasing in this period. In the stabilizing stage, when the space generated by the mortality of canopy trees is larger than the growth of canopy tree crown area, no trees are pushed to the lower layer and the lower layer trees start to enter the canopy layer and fill the space, leading to a sharp decrease in critical height (Fig. 3: b) and the mixing of different sized trees in the canopy layer. The CAI is decreasing as well because of the high mortality rates of the understory layer trees. As time goes on, the growth, regeneration, mortality, and space filling processes are equilibrated, and the forest structure is then stabilized.

The tallest plant height (Fig. 3: c) shows the height of the trees in the tallest cohort. It keeps growing as this cohort exists. The sharp decreases indicate the replacements by or merging with another shorter cohort because the density of trees in this cohort is very low (0.0001/ha in this case) or the similarity between the tallest and the second tallest is high. The total basal area (Fig. 3: d) is an index of the sum of all trees at a site. It keeps increasing during forest development and is equilibrated earlier than height and crown structure.

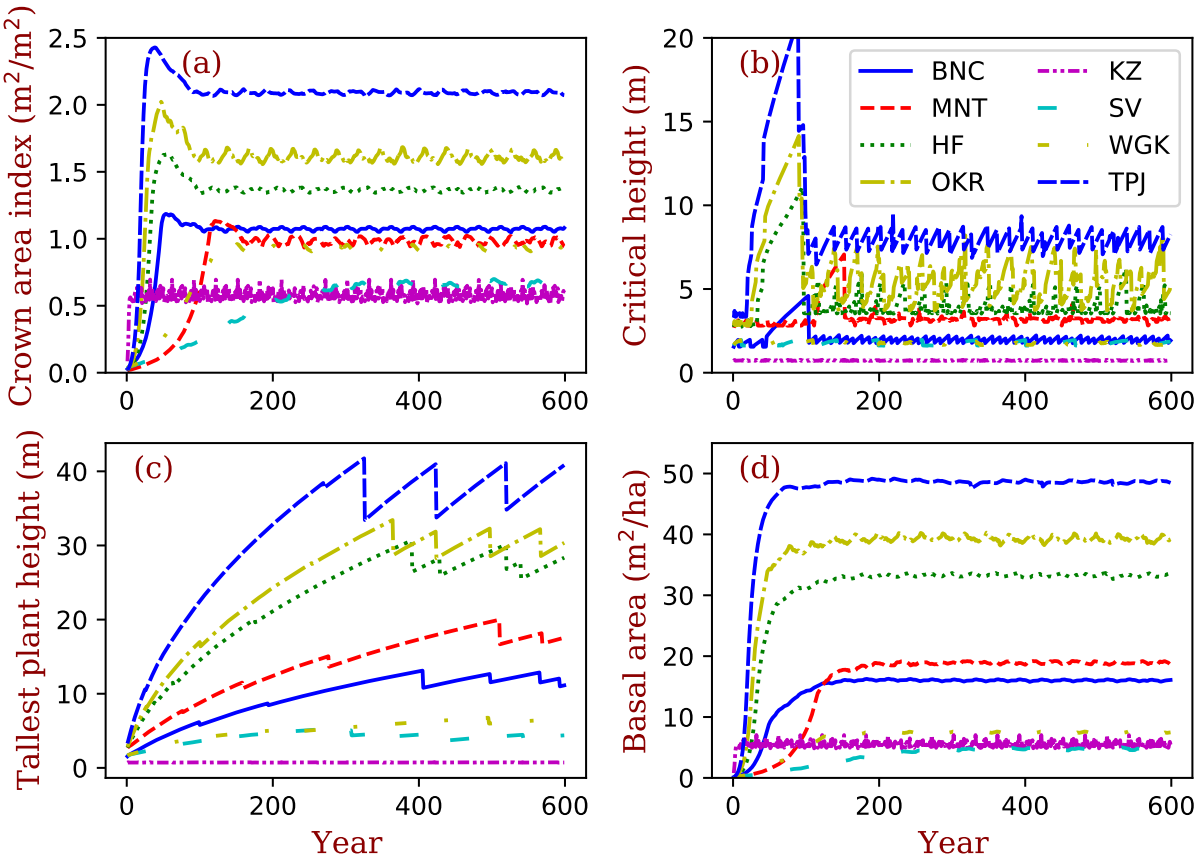

487

488 **Figure 3. Vegetation structural dynamics with the full demographic BiomeE.** Critical height
489 is an index of the model PPA, which separates the trees that are in full sunlight if taller than
490 critical height and those that are fully shaded if shorter than critical height.

491

492 Among these sites, at equilibrium, the tropical forest site (TPJ) has the highest crown area index
493 (around 2.2), followed by warm temperate forest at OKR, mixed forest at HF, and boreal forests
494 at BNC and MNT (Fig. 3). The shrubs and grasslands in arid regions have the lowest crown area
495 index (CAI), with basal area following similar patterns. For forested sites, tree height is tallest at
496 TPJ, followed by OKR, HF, MNT, and BNC. The shrubs are short according to their allometry
497 parameters and the height of grasses during non-growing season is zero. The critical height,
498 which separates canopy layer trees from the understory layers, follows the same order as that of

tree height with high fluctuations with cohort changes. (More cohort details are in Supplementary Information Figures S1-S8)

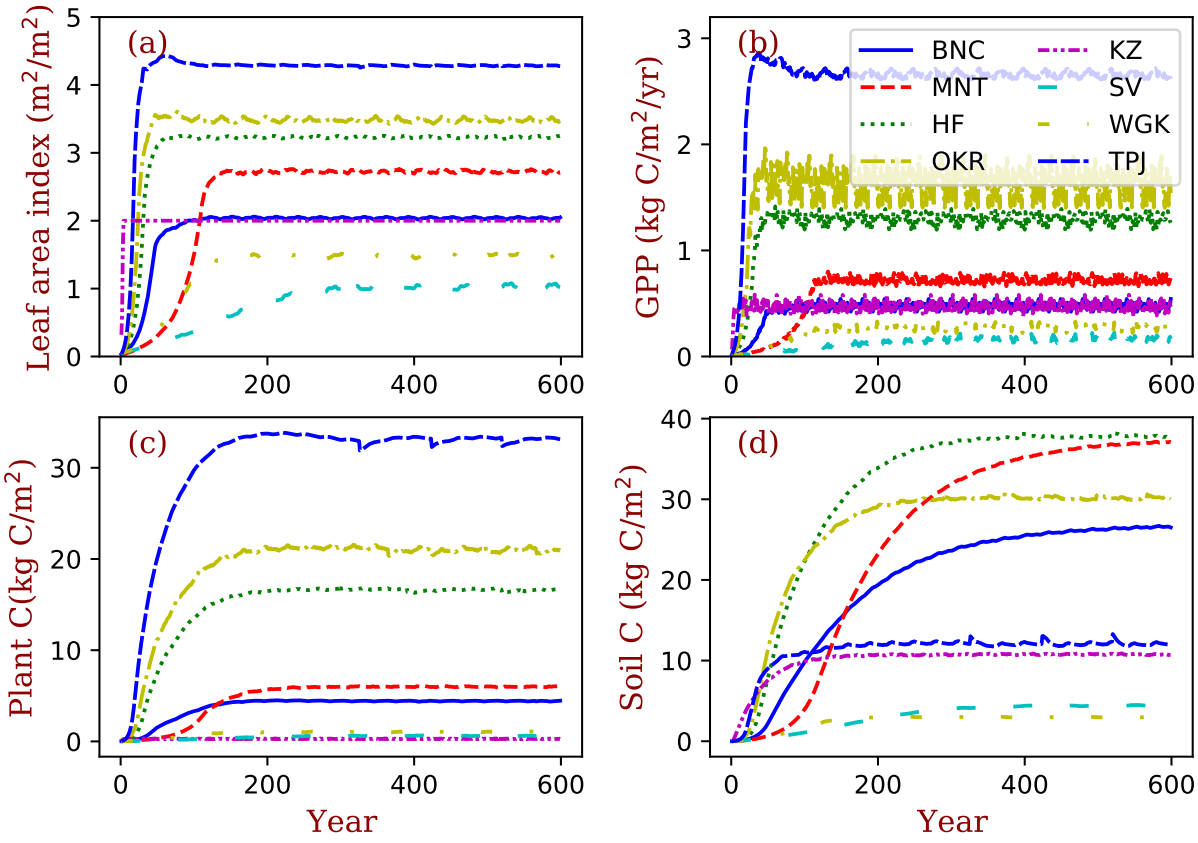

Figure 4: Site ecosystem development simulated by BiomeE with full demography

For the temporal dynamics in the full demographic simulations (Fig. 4), the simulated GPP aligns closely with LAI and they reach their equilibrium states at similar times across sites (Fig. 4: a,b). According to the definition of maximum crown LAI (l_{max}) in Eq. 6, the grass LAI (i.e., Konza) reaches the maximum each year, except the first year due to the low initial density (Fig. 4: a). The biomass accumulation is much slower in forests because of the longer time needed for forest structure (size distribution) to reach equilibrium. Soil carbon equilibration is faster in the warm regions than in cold regions overall because of the higher turnover rate of

SOM pools in warm regions. At equilibrium, forested sites have higher LAI, biomass, and carbon stocks per area compared to the shrub and grass sites overall. Vegetation biomass is lowest at the grassland site, Konza LTER, because, within the model, grassland ecosystems cannot accumulate persistent woody biomass.

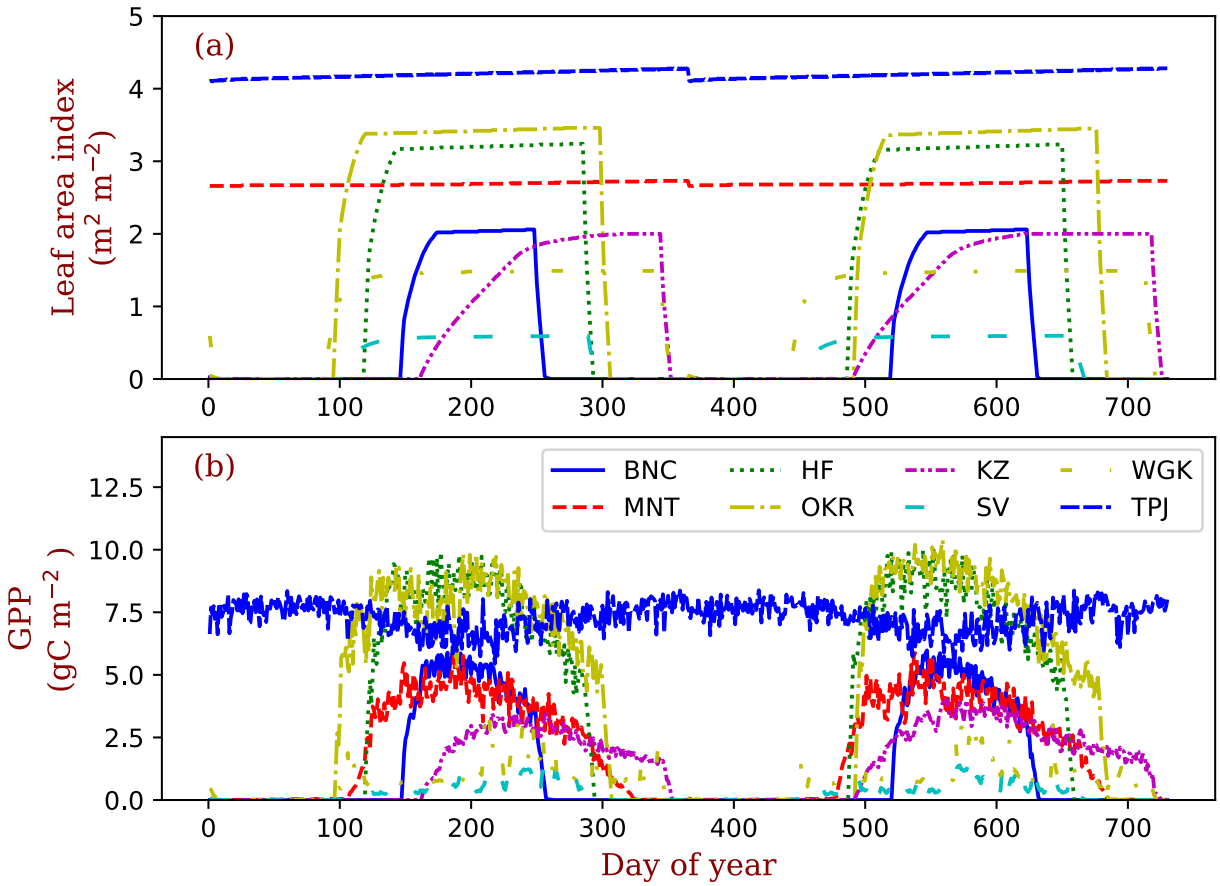

Figure 5. Seasonal patterns of LAI and gross primary production in the sample grids. Two years of data are shown in this figure. The key to location abbreviations is in Table 2.

The PFTs at TPJ and MNT are evergreen trees. Their LAI does not change over the whole year (Fig. 5: a). The forest in OKR has the longest growing season in the three deciduous forest grids, followed by HF and BNC. BNC's growing season is only around 120 days, about half of OKR's growing season. The growing season of grasses in KZ starts in late May and ends in September. The two arid-adapted shrub sites (SV and WKG) are controlled by water availability.

In TPJ (tropical evergreen forest), the trees have photosynthesis throughout the entire year (Fig. 5: b). In MNT, photosynthesis only happens in warm seasons with the leaves kept in the crowns (evergreen needleleaf). The deciduous trees in OKR and HF have high photosynthesis rates during the growing season. The photosynthesis rates in SV and WKG are generally low because of the dry environments. However, the precipitation events can drive photosynthesis rates high in these arid regions. At the global spatial scale, only evergreen needle-leaved forests keep their leaves in northern high latitude regions during January (Fig. 6), though photosynthesis in this region ceases because of the low temperature. In July, northern high latitude regions green up and their photosynthesis rates are high in wet regions. The single cohort BiomeE predicted similar pattern because the phenology model is same (Figure S9).

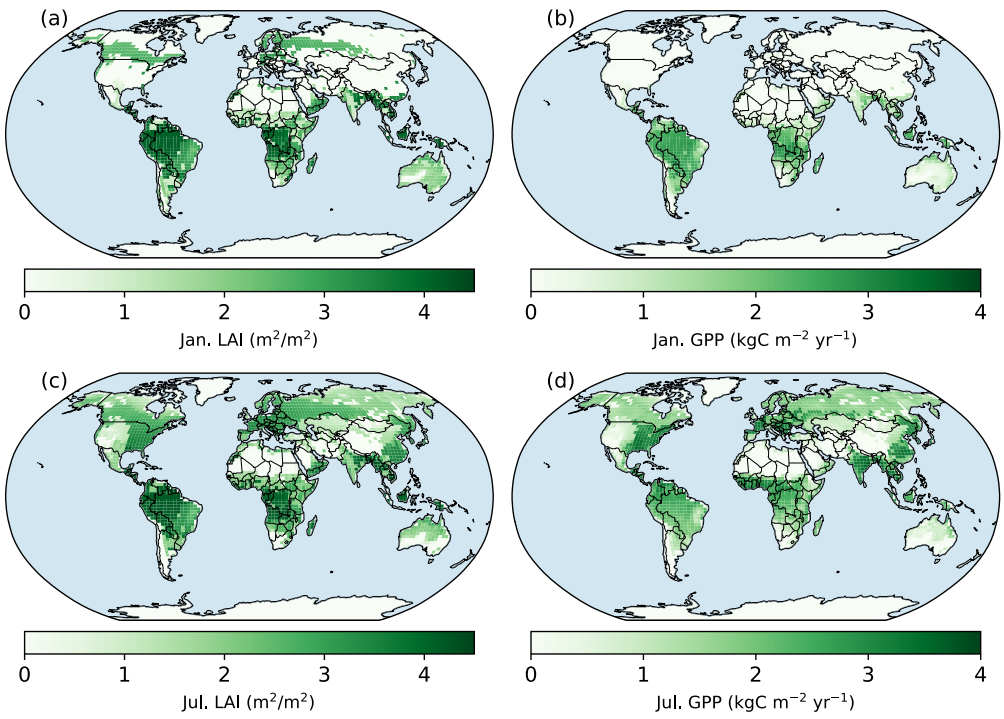

Figure 6. Spatial patterns of LAI and GPP in Jan and July simulated with full demography setting. Panels a and b are the LAI and photosynthesis of January in the year of 600 (the last year of model run). Panels c and d are July's in the same year.

4.2 Global Comparisons with Observations

We tuned the parameter of maximum carboxylation rate (V_{cmax}) to fit the general pattern of global GPP. Compared with SIF GPP (Alemohammad et al., 2017), simulated GPP is higher than the SIF GPP generally (Figs. 7 and 8), though lower in arid regions (Fig. 7). The simulated tree height is mostly taller compared to observations (Simard et al., 2011) because most forests have been altered by human activities (Pan et al., 2013). However, the model and observations cover approximately the same range of tree heights (up to 40 m). Simulated biomass is much higher than the observations because, in the observations, many forest regions have been transformed to low biomass land use types (such as croplands) or represent earlier successional stages with less accumulated carbon (i.e., not equilibrium states).

Simulated soil carbon does track the observations (Figure 7: g and h) better than biomass, likely because soil carbon stocks are more stable compared to biomass; and GPP does not change much compared to the changes in vegetation biomass because leaves can reach to equilibrium much faster than the biomass does (Fu et al., 2017). For areas where the model underpredicts soil carbon, the difference could arise from the missing biogeochemical processes that may lead to high carbon accumulation in some regions (e.g., peats) (Davidson and Janssens, 2006; Briones et al., 2014; Euskirchen et al., 2014) and the relatively high uncertainties in the soil carbon data (Tifafi et al., 2018).

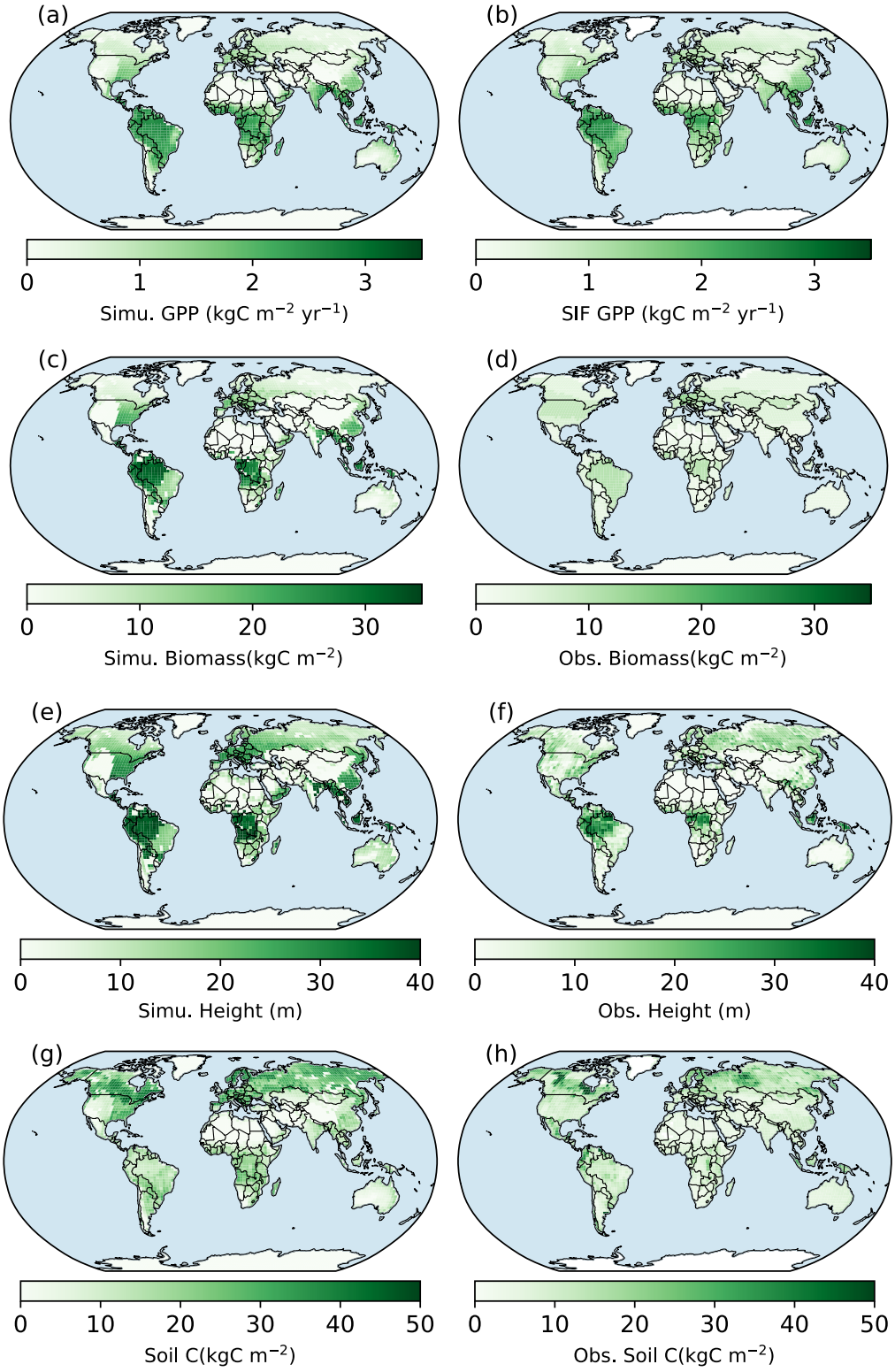

557

558

559 **Figure 7. Spatial patterns of BiomeE (full demography) simulations and those from data**.
560 "Obs." means different way retrieved from observations. Some are model-based (e.g., GPP is

from SIF data and tree height is from LiDAR data). Obs. **GPP is** derived from Solar Induced Fluorescence (SIF) data with a machine learning approach (Alemohammad et al., 2017). The data are available from Jan. 2007 to Dec. 2015. **The tree height data** are from spaceborne light detection and ranging (lidar) global map of canopy height at 1-km spatial resolution developed by Simard et al. (2011). **Biomass data** are from Hengeveld et al. (2015). **Soil carbon data** are from FAO Harmonized World Soil Database (version 1.2), updated by Wieder (2014).

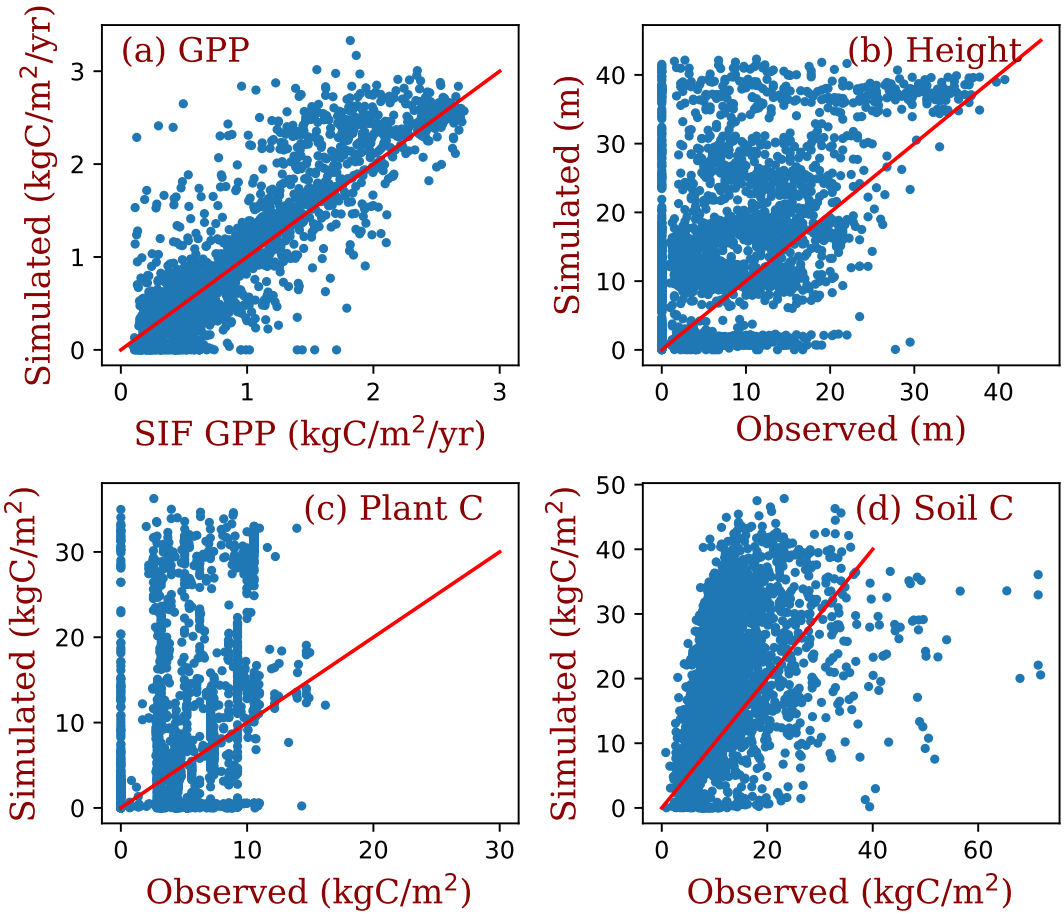

Figure 8. **Grid comparison of full demographic BiomeE simulations with observations estimates**. The red line in each panel is the 1:1 line. This figure uses the same simulated and observed data as those of Figure 7.

4.3 Comparison with MsTMIP models

We compared the performance of our model with MsTMIP models at the 8 locations that were used to show ecosystem development patterns (Table 2). For most of these sites, LAI in BiomeE is lower compared the other MsTMIP models (Fig. 9: a), while the estimated GPP is within the range of MsTMIP predictions (Fig. 9: b). LAI differences are a consequence of the formulations within BiomeE. Specifically, BiomeE simulates leaf growth by using a maximum crown LAI, which is lower than the real forest LAI.

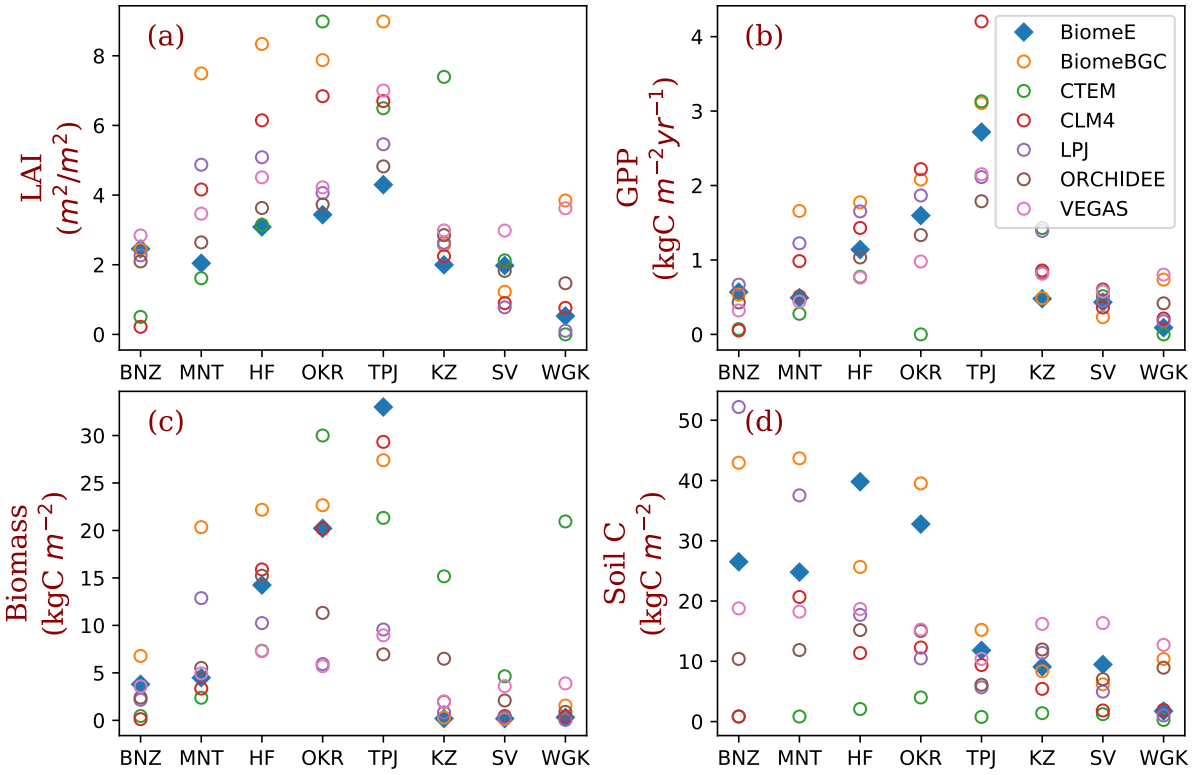

Figure 9 Site-level comparison with MsTMIP models.

The BiomeE predictions are from the full demography. The abbreviations of the 8 sites (corresponding to model grid cells) and their coordination, dominant PFTs, and climatic conditions are in Table 2. (See Figures S12 and S13 in Supplementary Information for the single cohort BiomeE simulations.)

The low LAI does not affect crown total photosynthesis because leaves in lower canopy layers contribute little to the total carbon assimilation. BiomeE predicted biomass (Fig. 9: c) and

soil carbon (Fig. 9: d) generally fall towards the higher end of the MsTMIP simulations, except for the more arid grass- and shrub-dominated sites. We note, however, that there are wide differences in estimates for vegetation and soil carbon across the models, likely because of different treatments of mortality and decomposition functions in these models.

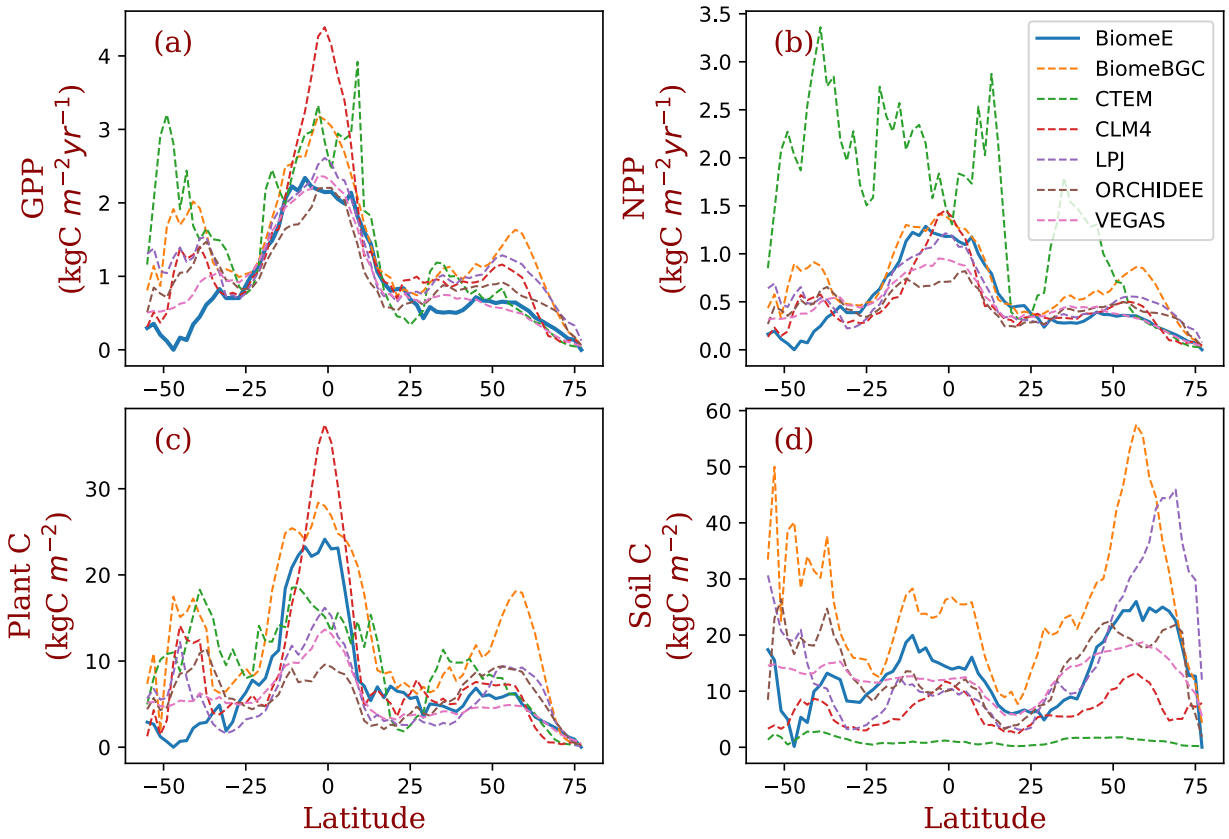

Figure 10 Latitudinal patterns of GPP, NPP, Biomass, and soil carbon as simulated by BiomeE (with full demography) and MsTMIP models

More broadly, the latitudinal mean of BiomeE simulated GPP is at the lower end of MsTMIP model predictions (Fig. 10: a). Since BiomeE's GPP was tuned to fit remote sensing data derived GPP, the MsTMIP models may over-estimate global GPP. BiomeE simulated NPP (Fig. 10: b), plant carbon (Fig. 10: c), and soil carbon (Fig. 10: d) are within the range simulated by the MsTMIP models. This indicates that BiomeE has slightly lower respiration than the MsTMIP

602 models. In the arid regions (e.g., around latitude 40-50 °S), our model's GPP is lower than

603 MsTMIP's because of sensitive drought responses in our model.

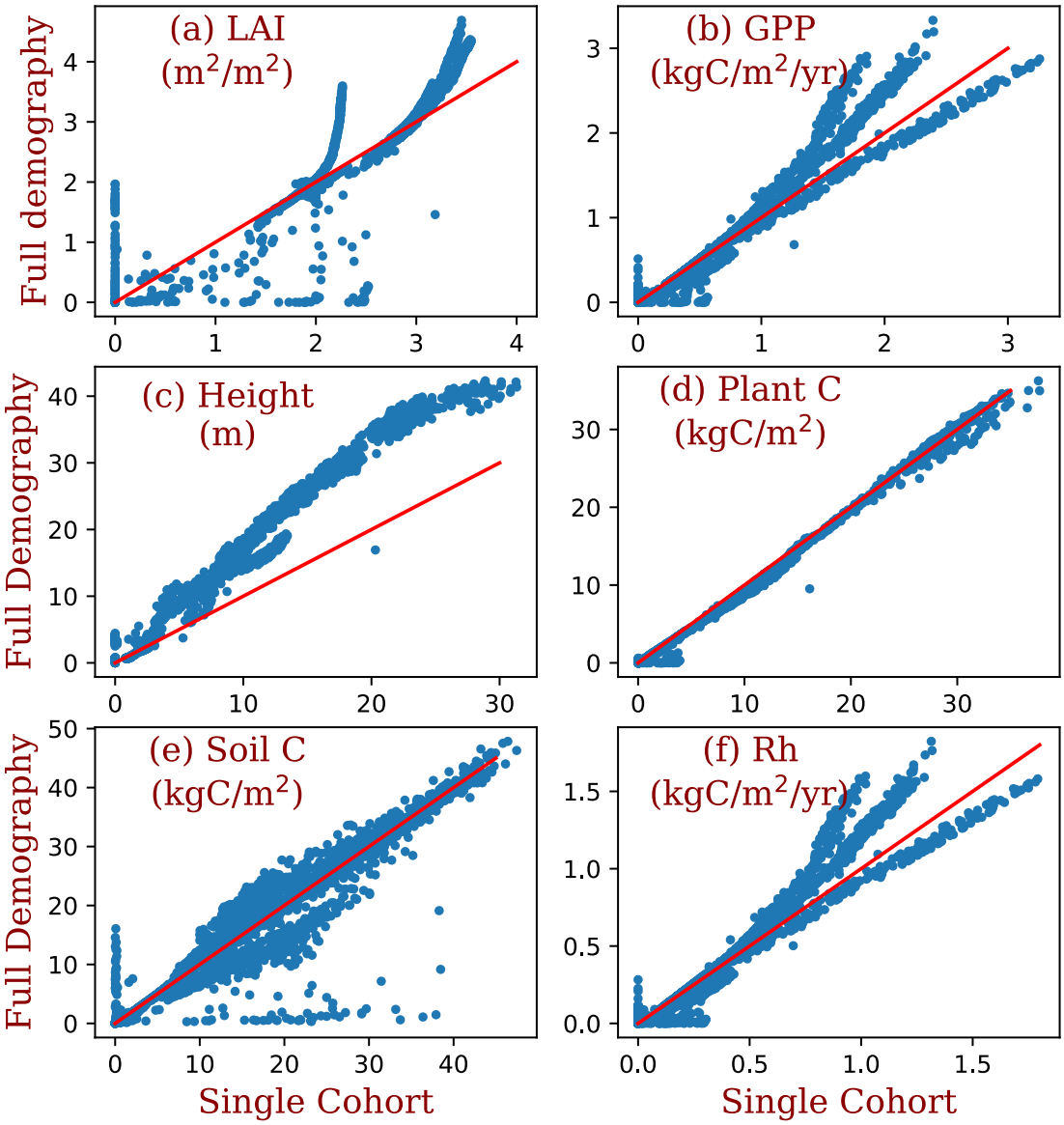

604

605 **Figure 11 Comparison between the simulations of the full demography and the single**
606 **cohort settings of BiomeE.**

607

608 The demographic processes have significant impacts on the simulations of GPP, biomass, soil

609 carbon, and vegetation structure compared to the single-cohort BiomeE (Figure 11). The full

demographic BiomeE includes an understory layer of plants, resulting in higher LAI in high LAI regions and also slightly higher GPP. Higher GPP in the model with full demography leads to a high allocation to leaves and fine roots. However, the total biomass predicted by the two model versions are similar because of the tradeoffs in allocation between leaves and stem growth and tree size distribution and because most biomass is concentrated in stems (Please refer to the Figures S10 and S11 in Supplementary Information for the single cohort BiomeE simulations). In the full demography model, tree mortality removes all the biomass, including leaves, fine roots, and stems, while in the single-cohort model, the mortality is represented as the turnover of woody biomass. Consequently, the full demography model has higher emergent turnover rate for the whole vegetation.

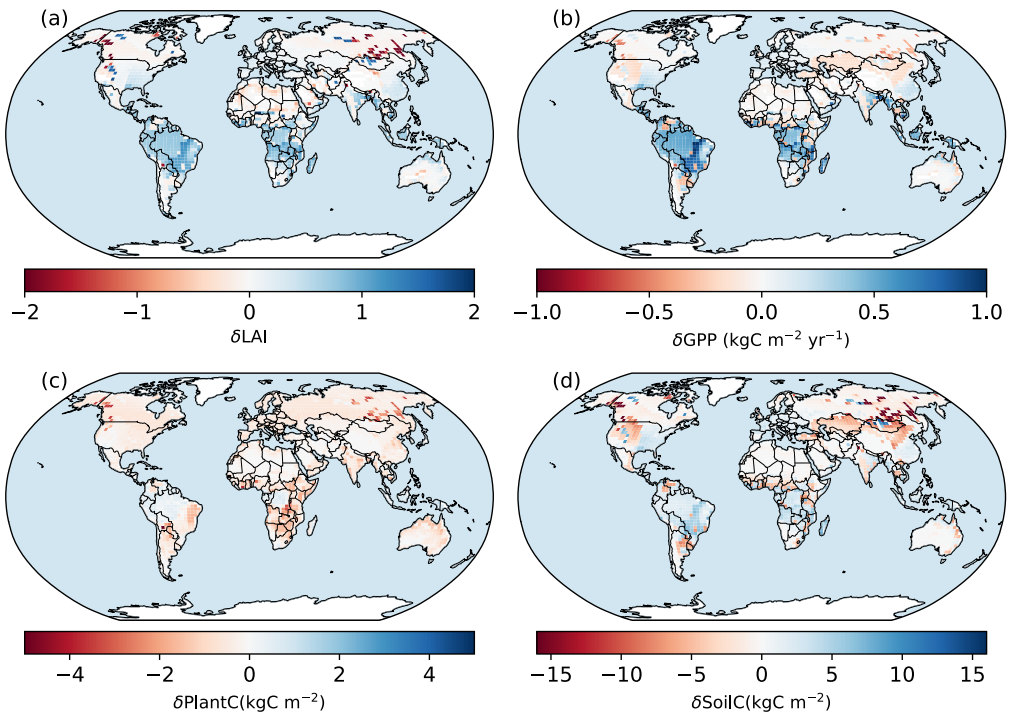

Figure 12 Spatial patterns of the differences between the simulations of the BiomeE: full demography minus the single-cohort simulations.

Compared to the single-cohort model, the full demography model predicts higher LAI and GPP in warm and wet regions and lower values in cold and dry regions (Fig. 12: a, b). The full demography model also predicts much lower biomass and soil carbon than the single-cohort model in cold and dry regions (Fig. 12: c). Because the single cohort model has the same SOM pools and turnover/decomposition processes, the reduced biomass input from full demography alone is causing the difference in SOM dynamics. This is consistent with the functions of demographic processes in these regions, which greatly reduce model stability because reproduction and survival are lower in dry and cold regions. By contrast, the single-cohort model does not simulate these processes explicitly and instead uses a simplified routine turnover of materials that allows plants to stay in extremely dry or cold conditions.

4.4 Eco-evolutionary simulation and sensitivity test

This model has the potential to predict competitively dominant PFTs in the continuum of plant traits through succession simulations according to the principles of evolutionarily optimal competition strategy. We illustrate this with a set of simulations conducted at a series of ecosystem nitrogen content (from 269 to 575 g N/m^2) with five PFTs sampled from the continuums of LMA (σ, from 0.06 to 0.14) and target root/leaf area ratio (φ_{RL}, from 0.8 to 1.2 corresponding to each LMA). The different ecosystem total nitrogen represents the environmental conditions that can result from soil and climate conditions. The simulations are set as nitrogen-closed (i.e., no input and output of nitrogen). At the lowest ecosystem total nitrogen (Fig. 13: a), the PFT with highest LMA (0.14 kg C/m^2 leaf) wins. With increases in ecosystem nitrogen (Fig. 13: b - d), the winner shifts to lower LMA PFTs. This means that in infertile soils or cold climates with slower biogeochemical cycles (e.g., tundra and boreal forests), the eco-

evolutionarily optimal PFTs should have high LMA leaves, and vice versa. This pattern is consistent with the predictions of a theoretical model derived in Weng et al. (2017). This simulation is also a case of sensitivity test of the simulated vegetation dynamics at environmental conditions. Vegetation can shift their compositions and dominant plant traits to maintain an eco-evolutionarily optimal state, and thus amplify or attenuate the responses of ecosystem carbon cycle to climate changes.

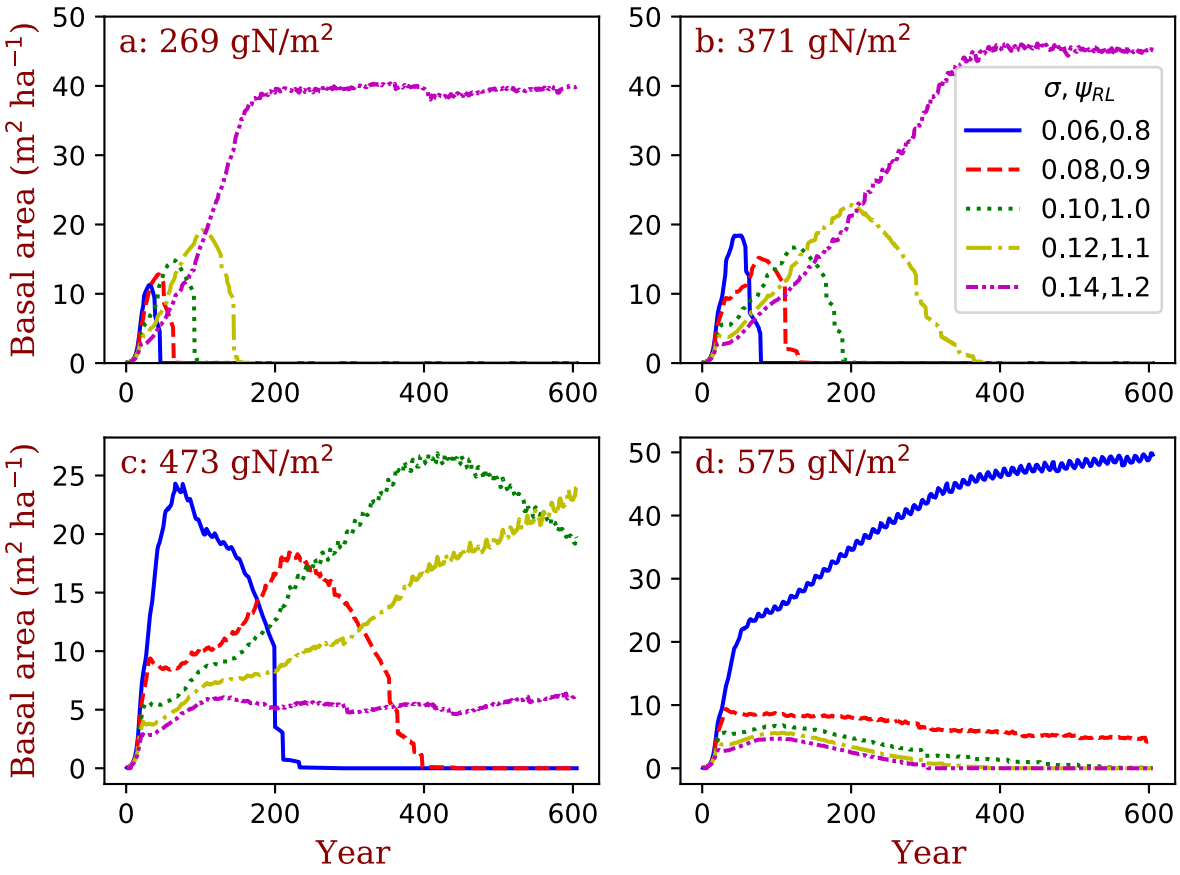

Figure 13. Simulated competitively dominant PFTs at different total ecosystem nitrogen. The simulations are set as nitrogen-closed (i.e., no input and output of nitrogen). The number in the title of each panel is the initial soil nitrogen. We used five PFTs that only differed in their LMA (σ) and target root/leaf area ratio (φ_{RL}) corresponding to each LMA in each simulation.

5 Discussion

We developed a parsimonious terrestrial ecosystem model for ModelE to simulate vegetation dynamics and ecosystem biogeochemical cycles. This model includes a cohort-based representation of vegetation structure, a height structured light competition scheme, demographic processes, and coupled carbon-nitrogen biogeochemical cycles. This model has four major modules that organize the hierarchical processes of ecosystems together into a cohesive modeling structure: 1) plant physiology (photosynthesis, respiration), 2) plant phenology and growth, 3) vegetation structural dynamics, and 4) soil biogeochemical cycles (Figure 1). Each module is cohesive and has a minimum set of variables as the input from other modules.

5.1 Model formulation

In designing this model, we considered the simulation of competitively optimal strategy of plants in different climates based on fundamental ecological rules (Purves and Pacala, 2008; Falster and Westoby, 2003; Franklin et al., 2020). These strategies are mainly related to light competition, water conditions, nutrient use efficiency, and disturbances (e.g., fire), and represented by the traits of wood density, height growth, leaf longevity, and photosynthesis pathways. PFTs are used in this model as an integrative unit representing combinations of plant traits for simulating (1) the spontaneous dynamics of carbon, water, and energy fluxes as the core functions of an ESM-based land model and (2) the transient vegetation structural and compositional dynamics and ecosystem biogeochemical cycles in response to climate variations.

We adopted a generic design for the PFTs in the BiomeE. Since the PFTs are samples of plant traits in their natural ranges, the numbers of PFTs are flexible, depending on what

strategies the users wish to test (as the test simulations in Figure 13). This approach substantially simplifies the parameterization of PFTs because it changes the parametrizations to the selections of strategies through choosing different trait values (i.e., parameters). Thus, the PFTs are adaptive and can change to each other in different climate zones, making it possible to reduce the number of PFTs while representing functional diversity and the optimal adaptation to climate conditions.

To represent the major variations in plant functional diversity, we chose four plant traits as the primary axes to define PFTs: wood density, leaf mass per unit area (LMA), height growth parameter, and leaf maximum carboxylation rate (V_{cmax}). Wood density is relatively conservative (Swenson and Enquist, 2007; Chave et al., 2009), mostly ranging from 200 to 500 kg C m^{-3}, while herbaceous stem density ranges from 400~600 kg C m^{-3} (Niklas, 1995). However, herbaceous stems are usually hollow, making the ratio of total biomass to its volume low, and grasses shed their stems each growing season, resulting in faster stem turnover. It is a strategic difference from woody plants, which keep the woody tissues to build up their trunks and thus display their leaves on top of trunks for light competition (Dieckmann et al., 2007; Falster and Westoby, 2003). LMA is the key leaf trait that determines leaf life longevity and leaf types (i.e., evergreen vs. deciduous)) (Osnas et al., 2013), and represents the strategy for the competition in different soil nutrient levels (Tilman, 1988; Reich, 2014; Weng et al., 2017) and resistance to stresses of water and temperature (Oliveira et al., 2021).

In this model, the phenological type is simulated as an emergent property of plant physiological processes and its strategy to deal with seasonal variations of temperature and water availability. We used three parameters – growing degree days (GDD), running mean daily temperature, and critical soil moisture – to define all possible phenological types. These three

parameters are widely used in a variety of phenology models (Sitch et al., 2003; Prentice et al., 1992; Arora and Boer, 2005). As for soil organic matter decomposition, the CASA model is currently used in ModelE; it has 13 pools with different transfer coefficients and turnover rates (Randerson et al., 1997; Potter et al., 1993, 2003). The models developed thereafter have more sophisticated processes, especially those of microbial activities and carbon use efficiency (Manzoni et al., 2010; Wieder et al., 2014; Wang and Goll, 2021). We chose an intermediate complexity scheme that has only two SOM pools but a functional microbial pool for decomposing SOM so that the dynamics of SOM's C:N ratio, carbon use efficiency, and nitrogen mineralization can be reasonably simulated while keeping the model structure parsimonious.

5.2 Model predictions and performance

This model has four relatively distinctive sets of simulated variables that are critical for model performance and calibration: 1) Stomatal conductance, photosynthesis, and respiration; 2) demographic rates (i.e., allocation, structural growth, mortality, and reproduction); 3) LAI, tree size, crown self-organization, and vegetation structure; 4) Soil carbon and nitrogen storage. In this paper, we only evaluated the carbon cycle in the model simulations, though the nitrogen cycle is also simulated in tandem with the carbon cycle in the model. We did not extensively tune model parameters to fit observations because the purpose of this paper is to describe the formulation of the model. The core processes of this model, e.g., photosynthesis, respiration, phenology, growth, allocation, demography, soil biogeochemical cycles, are from well-developed models and have been shown able to capture observational patterns. Data assimilation approaches can be implemented when parameter tuning becomes essential.

726 The simulations demonstrate that this model can capture global patterns of GPP, LAI, tree
727 height, biomass, and soil carbon, even though the parameters are not extensively tuned. For
728 example, global GPP patterns are consistent with those derived from SIF data (Fig.7: a, b and
729 Fig. 8: a), and simulated tree heights span the same ranges of those derived from data. The
730 simulated biomass and soil carbon is generally higher than in observations, though simulated soil
731 carbon is lower in some cold regions. Several factors likely explain the apparent overestimates of
732 GPP, biomass, and soil carbon in the model. First, the model uses a potential PFT distribution
733 and does not account for land cover change and land use history. For example, carbon dense
734 ecosystems (e.g., forests) have been extensively replaced by croplands and pastures. Second,
735 while vegetation in the real world reflects a variety of successional stages and the effect of
736 various disturbance events, our model analyses are based on equilibrium simulations without
737 explicit disturbances, such as fire, deforestation and regrowth. Third, the model assumes mineral
738 nitrogen is saturated and can consistently meet demands for plant growth. We did not fix the land
739 cover mismatches by compromising ecosystem physiological processes because we cannot put
740 all these effects into current model structure (i.e., mortality) when many processes are missing.

741 LAI is an illustrative variable for understanding why compromises are necessary when
742 integrating ecologically based vegetation models into ESMs. LAI, as a critical prognostic
743 variable in vegetation models, links both plant physiology and biogeophysical interactions with
744 climate systems. While LAI is usually simulated by a fixed allocation scheme, even if the
745 allocation ratios are dynamic with vegetation productivity (Montané et al., 2017), the prediction
746 of LAI in models is often simplified as the balance between growth and turnover. Modelers tend
747 to tune LAI to fit observations and get the required albedo and water fluxes whatever their
748 parameters of photosynthesis and respirations are. This LAI usually makes the lower layer

749 leaves carbon negative. However, a first principle is that a tree should have an optimal LAI to
750 maximize its carbon gain as a result of crown structure, light interception, and community-level
751 competition(Anten, 2002; Hikosaka and Anten, 2012; Niinemets and Anten, 2009). Thus, in our
752 model, because of the assumption of the uniform leaves within a crown, we defined a much
753 small target LAI to avoid carbon negative leaves.

754 The "uniform leaf" assumption makes the lower layer leaves carbon negative when LAI
755 is tuned close to that observed in tropical and boreal evergreen forests (where LAI is around
756 5~7). Therefore, the photosynthesis rate must be tuned to fit the canopy photosynthesis by
757 keeping the carbon negative leaves. However, the carbon negative leaves do not affect ecosystem
758 dynamics in the "single-cohort" models because the whole canopy net carbon gain is still
759 reasonable and can be fitted to the observed dynamics. This contrasts with the demographic
760 version of the model, which represents trees with different sizes and in different layers and
761 creates conditions where seedlings in the understory cannot survive because of light limitation
762 and negative carbon balances in some dry and cold regions. The leaf traits in the crown profile
763 should, in reality, be a function of light, water and nitrogen (Niinemets et al., 2015). A more
764 complex crown development module will then be required to simulate branching and leaf
765 development and deployment processes. Modelers should balance the model complexity and
766 computing efficiency then.

767 The leaf maximum carboxylation rate (V_{cmax}) used in this model is also much lower than
768 measured in young leaves (Bonan et al., 2011) because the aging of leaves is considered in the
769 mean value of V_{cmax} of all leaves with different ages. The mean V_{cmax} of the whole canopy leaves
770 is much lower than the new leaves that are usually used to measure V_{cmax}. If the leaves were not
771 specifically chosen, the mean of measured V_{cmax} is much lower than those used in models as

772 shown in Verryckt et al. (2022). This also indicates that V_{cmax} in current vegetation models is
773 over-estimated.

774 The allometry of plant architecture, rules for plant growth, and reproduction and mortality
775 processes form the basis of vegetation structural dynamics. The formulation of allometry makes
776 the whole-tree's photosynthesis and respiration proportional to crown area, and thus the growth
777 rate of tree diameter independent of crown area. The allocation scheme between the growth of
778 stems and functional tissues (i.e., leaves and fine roots) is the strategy of resources foraging for
779 light and soil resources, including height-structured competition for light. The vital rates drive
780 vegetation structural changes and biogeochemical cycles (Purves et al., 2008). Our model makes
781 it possible to simulate vegetation composition and structural dynamics based on the fundamental
782 principles of ecology, and the transient changes in terrestrial ecosystems in response to climate
783 change. This model therefore has the potential to predict competitively dominant strategies
784 represented by plastic plant traits (e.g., competitively dominant LMA in the simulations of Fig.
785 13), and the vegetation structure and composition that will be eco-evolutionarily optimized.

786

787 **5.3 Major uncertainties in BiomeE**

788 Global vegetation models typically require simplifying assumptions to organize
789 ecosystem processes at different scales into a cohesive model structure that balances the
790 complexity of ecosystem processes and the limitations of our knowledge (Prentice et al., 1992,
791 2007; Harrison et al., 2021). In our model, many processes, including phenology and drought
792 effects, are based on phenomenological equations representing the poorly understood links
793 between processes needed by the model to simulate the entire system. In the following sections,
794 we highlight these assumptions and evaluate their relative benefits and costs. Transparency in the

description of a community model such as this one will help future developers understand compromises and areas that can be improved with new information or approaches. The following phenomenological relationships represent the major sources of uncertainty in this model.

Water limitation of photosynthesis is calculated as a function of relative soil moisture following the water stress function from Rodriguez-Iturbe et al. (1999):

$$\beta_D = Min\left(1.0, max\left(\frac{s_D - s_{min}}{s^* - s_{min}}, 0.0\right)\right), \quad (16)$$

The parameters s^* and $s_{\min}$ are PFT-specific, representing different responses of PFTs to soil water conditions, and S_D is the relative soil moisture ranging from 0 (soil water content at wilting point) to 1 (at field capacity). This formulation that scales soil moisture to a scalar between zero to 1 is repeatedly used in both physiological responses of photosynthesis and phenology in ecosystem models as a simplistic treatment of the central role of water limitation on plant physiology (Harper et al., 2021; De Kauwe et al., 2015; Powell et al., 2013). This equation does not include the detailed processes of plant hydraulics and its adaptation to arid environments.

Plants have multiple tradeoffs and strategies to improve their competitiveness under water stress, such as regulating stomata conductance, shedding leaves, producing more roots, etc. (Oliveira et al., 2021; Volaire, 2018). At the ecosystem level, competition and evolutionary processes filter community emergent properties (Franklin et al., 2020; van der Molen et al., 2011). For example, trees in different climate regions have similar hydraulic safety margins (Choat et al., 2012), partly due to the intense competition for light (height growth) and water (root allocation) that require optimal use of available resources at any climate conditions (Gleason et al., 2017; Liu et al., 2019). However, in this model, the drought responses are only

delineated by Eq. 16. The parameter choices for s^* and s_{min} likely explain the amplified water stresses and low productivity in arid regions within our model.

Phenology represents the seasonal rhythms of plant physiological activities as adapted to periodic changes in temperature, precipitation, and light availability (Abramoff and Finzi, 2015; Caldararu et al., 2014; Chuine, 2010). DGVMs normally simulate leaf onset and senescence based on temperature conditions for cold deciduous plants and soil water conditions for drought deciduous plants (Arora and Boer, 2005; Caldararu et al., 2014). Phenology modeling is still highly empirical, although new models and approaches for cold deciduous and drought deciduous strategies have been proposed recently (e.g., Caldararu et al., 2014; Chen et al., 2016; Dahlin et al., 2015; Manzoni et al., 2015). We used a simple formulation of temperature (Eqs 1 and 3) and drought responses. For the cold-deciduous strategies, the phenology model balances growing season length and frost risks by adjusting critical GDD0 and T0 according to chilling days and growing days to reduce frost risk in warm regions and increase growing season length in cold regions. In this way, leaf senescence also considers growing season length and leaf aging. For example, in areas with longer growing seasons, plants will have a higher T0 and initiate senescence at higher temperatures. For the drought phenology, we set different critical soil moisture indexes to initiate and terminate a growing season (Table 1). However, these relationships are phenomenological, and ecological rules will benefit future model development.

Mortality is an integrative result of accumulative physiological stresses, structural damages, and disturbances during a tree's lifetime. The direct reasons can be starvation, structural failure, hydraulic failure, etc. (McDowell, 2011; Aakala et al., 2012; Aleixo et al., 2019). In this model, we only consider the background mortality and define its rate as a function

of tree diameter and light environment (Eq. 10). Hydraulic failure-induced mortality is required for studying plant responses to climate changes.

We employed these general phenomenological equations primarily because more mechanistic equations are not currently known. We are using the key variables that characterize ecosystem properties to define the basic model structure but have to use less-than-solid information to link them together by phenomenological relationships, as all the models do. In addition, our interest is to keep this model as simple as possible to improve interpretability and transparency and to reduce the computational burden when it is integrated into the ModelE. In these places where the tradeoff between model complexity and process accuracy is necessary, we highlight the underlying assumptions clearly, rather than implementing temporary fixes that lack solid ecological principles.

5.4 Insights from comparison with MsTMIP model

Most of the MsTMIP participant models have been analyzed by a model traceability method developed by Xia et al. (2013), which hierarchically decomposes model behavior into some fundamental processes of ecosystem carbon dynamics, such as GPP, carbon use efficiency (CUE), allocation coefficients, carbon residence time, carbon storage capacity, and environmental response functions (Zhou et al., 2021; Xia et al., 2013; Luo and Weng, 2011). This method is based on the assumptions of the linear system and the ecosystem emergent behavior per se (Emanuel and Killough, 1984; Eriksson, 1971; Sierra et al., 2018; Luo et al., 2012), making it is consistent with the concepts that are used as the basis of ecosystem carbon cycle models. The analyses of model traceability found, for the carbon cycle dynamics, the major uncertainty is from the modeling of the turnover rates (reciprocals of residence time) of

vegetation and soil carbon pools (Jiang et al., 2017; Chen et al., 2015). From CMIP5 to CMIP6, the modeling of NPP has been greatly improved, while the ecosystem carbon residence time remains highly biased (Wei et al., 2022).

According to the concepts of this traceability analysis approach (Xia et al., 2013), BiomeE also has a high uncertainty in the modeling of residence times of vegetation and soil carbon pools, because the mortality is picked up from the global forest data and the SOC decomposition processes are highly simplified. These issues have been discussed in the section of "5.3 Major uncertainties in BiomeE". These concepts (e.g., residence time, allocation coefficients) describe model emergent properties resulting from the underlying biological and ecological processes (i.e., micro-dynamics vs. macro-states). Fitting the emergent properties directly to improve model behavior is natural and convenient because many vegetation models are using these emergent properties (e.g., CUE, residence time, and allocation coefficients) to describe ecosystem processes in their formulations as a tradition of ecosystem modeling.

There are a couple of common and long-lasting issues in terrestrial ecosystem modeling, such as responses to warming, responses to atmospheric CO_2, drought stress effects, and vegetation compositional changes (Harrison et al., 2021; Franklin et al., 2020; Luo, 2007). These issues represent our knowledge gaps in ecosystem ecology. For modeling vegetation dynamics eco-evolutionarily, we need to use the fundamental ecological processes and unbreakable physical rules to simulate the emergent processes (e.g., Weng et al., 2019; Scheiter et al., 2013), With the design of vegetation modeling in the BiomeE, such as the explicit demographic processes, individual-based competition for different resources, and flexible trait combinations of PFTs, this model is able to predict some key emergent dynamics of ecosystems based on the underlying biological and evolutionary mechanisms (as shown in Figure 13). Data from field

883 experiments (Ainsworth and Long, 2004; Crowther et al., 2016), observatory networks (e.g.,
884 Fluxnet, Baldocchi et al., 2001; Friend et al., 2007), and remote sensing (Duncanson et al.,
885 2020), can provide direct information for modeling the underlying ecological processes and
886 validating predicted emergent properties.

887

888 **5.5 Model stability and complexity**

889 Ecosystem demographic processes (e.g., reproduction and mortality) are a source of high
890 sensitivity and uncertainty in BiomeE. In some environmental conditions, especially in dry or
891 cold regions, the predefined parameters can lead to high mortality or failure of reproduction,
892 making ecosystems highly instable. To understand these issues, we developed a "single-cohort"
893 version of the model to aid in the diagnosis of issues in the full demographic version of the
894 model. The major issue we identified is the fact that the model formulation is based on functional
895 processes in highly-productive regions, whereas the model is applied globally and across much
896 more diverse environmental conditions (e.g., arid environments). The variables and parameters
897 that work well in highly-productive regions (e.g., initial seedling sizes, default leaf growth,
898 minimum allocation ratios, etc.) are often unsuitable in regions with higher environmental stress.
899 And although plants have evolved special features to deal with more extreme conditions (Lloret
900 et al., 2012; Reyer et al., 2013; Singh et al., 2020), these features have not yet been integrated
901 into the model.

902 There is a tendency in current DGVMs to use individual plant physiological trait changes
903 to represent community shifts. This approach is usually characterized as "parameter dynamics"
904 or "response functions" (Fisher and Koven, 2020; Luo and Schuur, 2020) for reducing model
905 processes and complexity. Adding new processes to work around existing problems, instead of

redesigning the fundamental model processes, is common in model development. The approach is helpful for tracking model development, undoing wrong additions, and improving model performance. However, work-arounds often increase model complexity without concomitant improvements in model predictions.

Generally, a model's usefulness is improved by transparent assumptions, a well-defined model structure, and output that is testable against data (Famiglietti et al., 2021; Forster, 2017; Hourdin et al., 2017). Data assimilation approaches improve model parameterization more efficiently and effectively than manually tuning individual parameters (Williams et al., 2009; MacBean et al., 2016; Wang et al., 2009) and allow for more detailed uncertainty analysis (Luo et al., 2009; Weng et al., 2011; Weng and Luo, 2011; Xu et al., 2006; Dietze, 2014). It is important to only include necessary assumptions in a model and to include them in ways that do not compromise other processes or parameters. Modelers should try their best not to add poor-understood processes if not necessary. Additionally, many specifications of model formulation are based on the questions that a user is trying to answer in their research. We should not expect to develop an all-encompassing model that fits all application scenarios. On the contrary, maintaining model flexibility and transparency is critical for using this model as a tool to explore specific science questions. In BiomeE, we have opted for what we consider the most parsimonious and, at the same time, theoretically sound formulations of allometry, phenology, and allocation dynamics to allow for computational efficiency in capturing vegetation grown and ecological dynamics in the context of an ESM.

5.6 Legacy limitations of ModelE coding and development conventions

928 The legacy of model coding structure and the history of model development can greatly affect
929 the functions and the selection of model formulations (Alexander and Easterbrook, 2015).
930 ModelE was developed as a general circulation model, and vegetation in the model to date has
931 been represented with a simple set of static biophysics parameterizations to regulate exchanges
932 of energy and moisture between the land surface and the atmosphere (Hansen et al., 2007;
933 Schmidt et al., 2014; Kelley et al., 2020). To advance the functionality of the vegetation and the
934 land surface model within ModelE, increases in complexity must therefore be balanced with the
935 computational demands of the fully-coupled model.

936 In ModelE, the land model, TerraE, is used to calculate land surface (including vegetation)
937 water and energy fluxes and soil water dynamics based on the characteristics of vegetation
938 derived from the vegetation model (e.g., canopy conductance, wetness, etc.) at the grid scale. It
939 does not calculate each cohort's transpiration and water uptake. In our vegetation model, the
940 water limitation of stomatal conductance is calculated as a function of soil water stress index and
941 root vertical distribution, instead of the direct plant root water supply (plant hydraulics). This
942 setting works well for the big leaf model (one canopy at one grid). However, when multiple
943 cohorts of plants are represented, as we do in BiomeE, it is unable to represent water competition
944 and differentiate the contribution of each single cohort's contribution to the total transpiration. A
945 structural change will be required to solve this problem by calculating transpiration from the
946 bottom-up (i.e., from cohort up to grid cell).

947

948 **6 Conclusions**

949 We developed a new demographic vegetation model to improve the representation of terrestrial
950 vegetation dynamics and ecosystem biogeochemical cycles in the NASA Goddard Institute of

Space Studies' coupled Earth system model, ModelE. This model includes the processes of plant growth, mortality, reproduction, vegetation structural dynamics, and soil carbon and nitrogen cycling. To scale this model globally, we added a new set of plant functional types to represent global vegetation functional diversity and introduced new phenology algorithms to deal with the seasonality of temperature and soil water availability. Competition for light and soil resources is individual-based, which makes the modeling of eco-evolutionary optimality possible. This model predicts the dynamics of vegetation and soil biogeochemistry including leaf area index, vegetation structure (e.g., height, tree density, size distribution, crown organization), and ecosystem carbon and nitrogen storage and fluxes. This model will enable ModelE to simulate long-term biogeophysical and biogeochemical feedbacks between the climate system and land ecosystems at decadal to century temporal scales. It will also allow for the prediction of transient vegetation dynamics and eco-evolutionary community assemblage in response to future climate changes based on the fundamental ecological principles.

Code and data availability

The model codes have been coupled with NASA GISS ModelE and will be released with ModelE codes (https://www.giss.nasa.gov/tools/modelE/). The codes of BiomeE module are available at https://doi.org/10.5281/zenodo.6476152. The simulated data have been archived at Zenodo (https://doi.org/10.5281/zenodo.6480411).

Author contributions

EW coded the model and performed test runs and data analysis. EW and BIC wrote the first draft of the manuscript. BIC, MJP, SSM, NYK, and EW designed the functional coupling with ModelE and the land module. NYK, IA, RS, and MK contributed to input data, the IO structure and the coupling between BiomeE and ModelE. KW, RD, CE, and SWP contributed to conceptual model development and PFT design. All co-authors contributed to writing or improving the manuscript.

Competing interests

The authors declare that they have no conflict of interest.

Acknowledgements

This work was supported by NASA Modeling, Analysis, and Prediction (MAP) Program (award numbers: 80NSSC21K1496, NNH10ZDA001N, and 16-MAP16-0149). Computing resources for the model runs were provided by the NASA High-End Computing (HEC) Program through the NASA Center for Climate Simulation (NCCS) at Goddard Space Flight Center. We thank Dr. Pierre Gentine of Department of Earth and Environmental Engineering, Columbia University, for his help in GPP data and model validation.

990 **Reference**

991 Aakala, T., Fraver, S., Palik, B. J., and D'Amato, A. W.: Spatially random mortality in old-
992 growth red pine forests of northern Minnesota, 42, 899–907, https://doi.org/10.1139/x2012-
993 044, 2012.

994 Abramoff, R. Z. and Finzi, A. C.: Are above- and below-ground phenology in sync?, 205, 1054–
995 1061, https://doi.org/10.1111/nph.13111, 2015.

996 Ainsworth, E. A. and Long, S. P.: What have we learned from 15 years of free-air CO2
997 enrichment (FACE)? A meta-analytic review of the responses of photosynthesis, canopy
998 properties and plant production to rising CO2: Tansley review, 165, 351–372,
999 https://doi.org/10.1111/j.1469-8137.2004.01224.x, 2004.

1000 Aleixo, I., Norris, D., Hemerik, L., Barbosa, A., Prata, E., Costa, F., and Poorter, L.: Amazonian
1001 rainforest tree mortality driven by climate and functional traits, 9, 384–388,
1002 https://doi.org/10.1038/s41558-019-0458-0, 2019.

1003 Alemohammad, S. H., Fang, B., Konings, A. G., Aires, F., Green, J. K., Kolassa, J., Miralles, D.,
1004 Prigent, C., and Gentine, P.: Water, Energy, and Carbon with Artificial Neural Networks
1005 (WECANN): a statistically based estimate of global surface turbulent fluxes and gross
1006 primary productivity using solar-induced fluorescence, 14, 4101–4124,
1007 https://doi.org/10.5194/bg-14-4101-2017, 2017.

1008 Alexander, K. and Easterbrook, S. M.: The software architecture of climate models: a graphical
1009 comparison of CMIP5 and EMICAR5 configurations, 8, 1221–1232,
1010 https://doi.org/10.5194/gmd-8-1221-2015, 2015.

1011 Allen, C. D., Macalady, A. K., Chenchouni, H., Bachelet, D., McDowell, N., Vennetier, M.,
1012 Kitzberger, T., Rigling, A., Breshears, D. D., Hogg, E. H. (Ted), Gonzalez, P., Fensham,
1013 R., Zhang, Z., Castro, J., Demidova, N., Lim, J.-H., Allard, G., Running, S. W., Semerci,
1014 A., and Cobb, N.: A global overview of drought and heat-induced tree mortality reveals
1015 emerging climate change risks for forests, 259, 660–684,
1016 https://doi.org/10.1016/j.foreco.2009.09.001, 2010.

1017 Anderegg, W. R. L., Kane, J. M., and Anderegg, L. D. L.: Consequences of widespread tree
1018 mortality triggered by drought and temperature stress, 3, 30–36,
1019 https://doi.org/10.1038/nclimate1635, 2012.

1020 Anten, N. P.: Evolutionarily stable leaf area production in plant populations, 217, 15–32, 2002.

1021 Argles, A. P. K., Moore, J. R., Huntingford, C., Wiltshire, A. J., Harper, A. B., Jones, C. D., and
1022 Cox, P. M.: Robust Ecosystem Demography (RED version 1.0): a parsimonious approach
1023 to modelling vegetation dynamics in Earth system models, 13, 4067–4089,
1024 https://doi.org/10.5194/gmd-13-4067-2020, 2020.

1025 Arora, V. K. and Boer, G. J.: A parameterization of leaf phenology for the terrestrial ecosystem
1026 component of climate models, 11, 39–59, https://doi.org/10.1111/j.1365-
1027 2486.2004.00890.x, 2005.

1028 Arora, V. K., Katavouta, A., Williams, R. G., Jones, C. D., Brovkin, V., Friedlingstein, P.,
1029 Schwinger, J., Bopp, L., Boucher, O., Cadule, P., Chamberlain, M. A., Christian, J. R.,
1030 Delire, C., Fisher, R. A., Hajima, T., Ilyina, T., Joetzjer, E., Kawamiya, M., Koven, C. D.,

Krasting, J. P., Law, R. M., Lawrence, D. M., Lenton, A., Lindsay, K., Pongratz, J., Raddatz, T., Séférian, R., Tachiiri, K., Tjiputra, J. F., Wiltshire, A., Wu, T., and Ziehn, T.: Carbon–concentration and carbon–climate feedbacks in CMIP6 models and their comparison to CMIP5 models, 17, 4173–4222, https://doi.org/10.5194/bg-17-4173-2020, 2020.

Avissar, R. and Werth, D.: Global Hydroclimatological Teleconnections Resulting from Tropical Deforestation, J. Hydrometeor., 6, 134–145, https://doi.org/10.1175/JHM406.1, 2005.

Baldocchi, D., Falge, E., Gu, L., Olson, R., Hollinger, D., Running, S., Anthoni, P., Bernhofer, C., Davis, K., Evans, R., Fuentes, J., Goldstein, A., Katul, G., Law, B., Lee, X., Malhi, Y., Meyers, T., Munger, W., Oechel, W., Paw U, K. T., Pilegaard, K., Schmid, H. P., Valentini, R., Verma, S., Vesala, T., Wilson, K., and Wofsy, S.: FLUXNET: A New Tool to Study the Temporal and Spatial Variability of Ecosystem-Scale Carbon Dioxide, Water Vapor, and Energy Flux Densities, Bull. Amer. Meteor. Soc., 82, 2415–2434, https://doi.org/10.1175/1520-0477(2001)082<2415:FANTTS>2.3.CO;2, 2001.

Bonan, G. B., Lawrence, P. J., Oleson, K. W., Levis, S., Jung, M., Reichstein, M., Lawrence, D. M., and Swenson, S. C.: Improving canopy processes in the Community Land Model version 4 (CLM4) using global flux fields empirically inferred from FLUXNET data, 116, https://doi.org/10.1029/2010JG001593, 2011.

Brando, P. M., Paolucci, L., Ummenhofer, C. C., Ordway, E. M., Hartmann, H., Cattau, M. E., Rattis, L., Medjibe, V., Coe, M. T., and Balch, J.: Droughts, Wildfires, and Forest Carbon Cycling: A Pantropical Synthesis, Annu. Rev. Earth Planet. Sci., 47, 555–581, https://doi.org/10.1146/annurev-earth-082517-010235, 2019.

Briones, M. J. I., McNamara, N. P., Poskitt, J., Crow, S. E., and Ostle, N. J.: Interactive biotic and abiotic regulators of soil carbon cycling: evidence from controlled climate experiments on peatland and boreal soils, 20, 2971–2982, https://doi.org/10.1111/gcb.12585, 2014.

Brodribb, T. J., Powers, J., Cochard, H., and Choat, B.: Hanging by a thread? Forests and drought, 368, 261–266, https://doi.org/10.1126/science.aat7631, 2020.

Caldararu, S., Purves, D. W., and Palmer, P. I.: Phenology as a strategy for carbon optimality: a global model, 11, 763–778, https://doi.org/10.5194/bg-11-763-2014, 2014.

Chave, J., Coomes, D., Jansen, S., Lewis, S. L., Swenson, N. G., and Zanne, A. E.: Towards a worldwide wood economics spectrum, 12, 351–366, https://doi.org/10.1111/j.1461-0248.2009.01285.x, 2009.

Chen, M., Melaas, E. K., Gray, J. M., Friedl, M. A., and Richardson, A. D.: A new seasonal-deciduous spring phenology submodel in the Community Land Model 4.5: impacts on carbon and water cycling under future climate scenarios, 22, 3675–3688, https://doi.org/10.1111/gcb.13326, 2016.

Chen, Y., Xia, J., Sun, Z., Li, J., Luo, Y., Gang, C., and Wang, Z.: The role of residence time in diagnostic models of global carbon storage capacity: model decomposition based on a traceable scheme, Sci Rep, 5, 16155, https://doi.org/10.1038/srep16155, 2015.

Choat, B., Jansen, S., Brodribb, T. J., Cochard, H., Delzon, S., Bhaskar, R., Bucci, S. J., Feild, T. S., Gleason, S. M., Hacke, U. G., Jacobsen, A. L., Lens, F., Maherali, H., Martínez-Vilalta, J., Mayr, S., Mencuccini, M., Mitchell, P. J., Nardini, A., Pittermann, J., Pratt, R. B.,

Sperry, J. S., Westoby, M., Wright, I. J., and Zanne, A. E.: Global convergence in the vulnerability of forests to drought, https://doi.org/10.1038/nature11688, 2012.

Chuine, I.: Why does phenology drive species distribution?, 365, 3149–3160, https://doi.org/10.1098/rstb.2010.0142, 2010.

Clark, J. S., Iverson, L., Woodall, C. W., Allen, C. D., Bell, D. M., Bragg, D. C., D'Amato, A. W., Davis, F. W., Hersh, M. H., Ibanez, I., Jackson, S. T., Matthews, S., Pederson, N., Peters, M., Schwartz, M. W., Waring, K. M., and Zimmermann, N. E.: The impacts of increasing drought on forest dynamics, structure, and biodiversity in the United States, 22, 2329–2352, https://doi.org/10.1111/gcb.13160, 2016.

Crowther, T. W., Todd-Brown, K. E. O., Rowe, C. W., Wieder, W. R., Carey, J. C., Machmuller, M. B., Snoek, B. L., Fang, S., Zhou, G., Allison, S. D., Blair, J. M., Bridgham, S. D., Burton, A. J., Carrillo, Y., Reich, P. B., Clark, J. S., Classen, A. T., Dijkstra, F. A., Elberling, B., Emmett, B. A., Estiarte, M., Frey, S. D., Guo, J., Harte, J., Jiang, L., Johnson, B. R., Kröel-Dulay, G., Larsen, K. S., Laudon, H., Lavallee, J. M., Luo, Y., Lupascu, M., Ma, L. N., Marhan, S., Michelsen, A., Mohan, J., Niu, S., Pendall, E., Peñuelas, J., Pfeifer-Meister, L., Poll, C., Reinsch, S., Reynolds, L. L., Schmidt, I. K., Sistla, S., Sokol, N. W., Templer, P. H., Treseder, K. K., Welker, J. M., and Bradford, M. A.: Quantifying global soil carbon losses in response to warming, 540, 104–108, https://doi.org/10.1038/nature20150, 2016.

Dahlin, K. M., Fisher, R. A., and Lawrence, P. J.: Environmental drivers of drought deciduous phenology in the Community Land Model, 12, 5061–5074, https://doi.org/10.5194/bg-12-5061-2015, 2015.

Davidson, E. A. and Janssens, I. A.: Temperature sensitivity of soil carbon decomposition and feedbacks to climate change, Nature, 440, 165–173, https://doi.org/10.1038/nature04514, 2006.

De Kauwe, M. G., Zhou, S.-X., Medlyn, B. E., Pitman, A. J., Wang, Y.-P., Duursma, R. A., and Prentice, I. C.: Do land surface models need to include differential plant species responses to drought? Examining model predictions across a mesic-xeric gradient in Europe, 12, 7503–7518, https://doi.org/10.5194/bg-12-7503-2015, 2015.

Dieckmann, U., Brannstrom, A., HilleRisLambes, R., and Ito, H. C.: The Adaptive Dynamics of Community Structure, in: Mathematics for Ecology and Environmental Sciences, edited by: Takeuchi, Yasuhiro, Iwasa, Yoh, and Sato, Kazunori, Springer, 145–177, 2007.

Dietze, M. C.: Gaps in knowledge and data driving uncertainty in models of photosynthesis, 119, 3–14, https://doi.org/10.1007/s11120-013-9836-z, 2014.

Duncanson, L., Neuenschwander, A., Hancock, S., Thomas, N., Fatoyinbo, T., Simard, M., Silva, C. A., Armston, J., Luthcke, S. B., Hofton, M., Kellner, J. R., and Dubayah, R.: Biomass estimation from simulated GEDI, ICESat-2 and NISAR across environmental gradients in Sonoma County, California, Remote Sensing of Environment, 242, 111779, https://doi.org/10.1016/j.rse.2020.111779, 2020.

Dybzinski, R., Farrior, C., Wolf, A., Reich, P. B., and Pacala, S. W.: Evolutionarily Stable Strategy Carbon Allocation to Foliage, Wood, and Fine Roots in Trees Competing for

Light and Nitrogen: An Analytically Tractable, Individual-Based Model and Quantitative Comparisons to Data, 177, 153–166, https://doi.org/10.1086/657992, 2011.

Dybzinski, R., Farrior, C. E., and Pacala, S. W.: Increased forest carbon storage with increased atmospheric CO2 despite nitrogen limitation: a game-theoretic allocation model for trees in competition for nitrogen and light, 21, 1182–1196, https://doi.org/10.1111/gcb.12783, 2015.

Emanuel, W. R. and Killough, G. G.: Modeling terrestrial ecosystems in the global carbon cycle with Shifts in carbon storage capacity by land-use change, 65, 970–983, https://doi.org/10.2307/1938069, 1984.

Eriksson, E.: Compartment Models and Reservoir Theory, 2, 67–84, https://doi.org/10.1146/annurev.es.02.110171.000435, 1971.

Euskirchen, E. S., Edgar, C. W., Turetsky, M. R., Waldrop, M. P., and Harden, J. W.: Differential response of carbon fluxes to climate in three peatland ecosystems that vary in the presence and stability of permafrost, 119, 1576–1595, https://doi.org/10.1002/2014JG002683, 2014.

Falster, D. and Westoby, M.: Plant height and evolutionary games, 18, 337–343, https://doi.org/10.1016/S0169-5347(03)00061-2, 2003.

Falster, D. S., Braennstroem, A., Westoby, M., and Dieckmann, U.: Multitrait successional forest dynamics enable diverse competitive coexistence, 114, E2719–E2728, https://doi.org/10.1073/pnas.1610206114, 2017.

Famiglietti, C. A., Smallman, T. L., Levine, P. A., Flack-Prain, S., Quetin, G. R., Meyer, V., Parazoo, N. C., Stettz, S. G., Yang, Y., Bonal, D., Bloom, A. A., Williams, M., and Konings, A. G.: Optimal model complexity for terrestrial carbon cycle prediction, 18, 2727–2754, https://doi.org/10.5194/bg-18-2727-2021, 2021.

Farrior, C. E.: Theory predicts plants grow roots to compete with only their closest neighbours, Proceedings of the Royal Society B: Biological Sciences, 286, 20191129, https://doi.org/10.1098/rspb.2019.1129, 2019.

Farrior, C. E., Dybzinski, R., Levin, S. A., and Pacala, S. W.: Competition for Water and Light in Closed-Canopy Forests: A Tractable Model of Carbon Allocation with Implications for Carbon Sinks, 181, 314–330, https://doi.org/10.1086/669153, 2013.

Fisher, R. A. and Koven, C. D.: Perspectives on the Future of Land Surface Models and the Challenges of Representing Complex Terrestrial Systems, 12, e2018MS001453, https://doi.org/10.1029/2018MS001453, 2020.

Fisher, R. A., Muszala, S., Verteinstein, M., Lawrence, P., Xu, C., McDowell, N. G., Knox, R. G., Koven, C., Holm, J., Rogers, B. M., Spessa, A., Lawrence, D., and Bonan, G.: Taking off the training wheels: the properties of a dynamic vegetation model without climate envelopes, CLM4.5(ED), 8, 3593–3619, https://doi.org/10.5194/gmd-8-3593-2015, 2015.

Forster, P.: Half a century of robust climate models, 545, 296–297, https://doi.org/10.1038/545296a, 2017.

Franklin, O., Johansson, J., Dewar, R. C., Dieckmann, U., McMurtrie, R. E., Brannstrom, A., and Dybzinski, R.: Modeling carbon allocation in trees: a search for principles, 32, 648–666, https://doi.org/10.1093/treephys/tpr138, 2012.

Franklin, O., Harrison, S. P., Dewar, R., Farrior, C. E., Brännström, Å., Dieckmann, U., Pietsch, S., Falster, D., Cramer, W., Loreau, M., Wang, H., Mäkelä, A., Rebel, K. T., Meron, E., Schymanski, S. J., Rovenskaya, E., Stocker, B. D., Zaehle, S., Manzoni, S., van Oijen, M., Wright, I. J., Ciais, P., van Bodegom, P. M., Peñuelas, J., Hofhansl, F., Terrer, C., Soudzilovskaia, N. A., Midgley, G., and Prentice, I. C.: Organizing principles for vegetation dynamics, 1–10, https://doi.org/10.1038/s41477-020-0655-x, 2020.

Friedl, M. A., Sulla-Menashe, D., Tan, B., Schneider, A., Ramankutty, N., Sibley, A., and Huang, X.: MODIS Collection 5 global land cover: Algorithm refinements and characterization of new datasets, 114, 168–182, https://doi.org/10.1016/j.rse.2009.08.016, 2010.

Friedlingstein, P., Meinshausen, M., Arora, V. K., Jones, C. D., Anav, A., Liddicoat, S. K., and Knutti, R.: Uncertainties in CMIP5 Climate Projections due to Carbon Cycle Feedbacks, 27, 511–526, https://doi.org/10.1175/JCLI-D-12-00579.1, 2014.

Friend, A. D., Stevens, A. K., Knox, R. G., and Cannell, M. G. R.: A process-based, terrestrial biosphere model of ecosystem dynamics (Hybrid v3.0), Ecological Modelling, 95, 249–287, https://doi.org/10.1016/S0304-3800(96)00034-8, 1997.

Friend, A. D., Arneth, A., Kiang, N. Y., Lomas, M., Ogee, J., Roedenbeckk, C., Running, S. W., Santaren, J.-D., Sitch, S., Viovy, N., Woodward, F. I., and Zaehle, S.: FLUXNET and modelling the global carbon cycle, 13, 610–633, https://doi.org/10.1111/j.1365-2486.2006.01223.x, 2007.

Fu, Z., Li, D., Hararuk, O., Schwalm, C., Luo, Y., Yan, L., and Niu, S.: Recovery time and state change of terrestrial carbon cycle after disturbance, Environ. Res. Lett., 12, 104004, https://doi.org/10.1088/1748-9326/aa8a5c, 2017.

Garcia, E. S., Swann, A. L. S., Villegas, J. C., Breshears, D. D., Law, D. J., Saleska, S. R., and Stark, S. C.: Synergistic Ecoclimate Teleconnections from Forest Loss in Different Regions Structure Global Ecological Responses, PLoS One, 11, https://doi.org/10.1371/journal.pone.0165042, 2016.

Gleason, K. E., Bradford, J. B., Bottero, A., D'Amato, A. W., Fraver, S., Palik, B. J., Battaglia, M. A., Iverson, L., Kenefic, L., and Kern, C. C.: Competition amplifies drought stress in forests across broad climatic and compositional gradients, 8, e01849, https://doi.org/10.1002/ecs2.1849, 2017.

Green, J. K., Konings, A. G., Alemohammad, S. H., Berry, J., Entekhabi, D., Kolassa, J., Lee, J.-E., and Gentine, P.: Regionally strong feedbacks between the atmosphere and terrestrial biosphere, Nature Geosci, 10, 410–414, https://doi.org/10.1038/ngeo2957, 2017.

Hansen, J., Sato, M., Ruedy, R., Kharecha, P., Lacis, A., Miller, R., Nazarenko, L., Lo, K., Schmidt, G. A., Russell, G., Aleinov, I., Bauer, S., Baum, E., Cairns, B., Canuto, V., Chandler, M., Cheng, Y., Cohen, A., Del Genio, A., Faluvegi, G., Fleming, E., Friend, A., Hall, T., Jackman, C., Jonas, J., Kelley, M., Kiang, N. Y., Koch, D., Labow, G., Lerner, J., Menon, S., Novakov, T., Oinas, V., Perlwitz, Ja., Perlwitz, Ju., Rind, D., Romanou, A.,

Schmunk, R., Shindell, D., Stone, P., Sun, S., Streets, D., Tausnev, N., Thresher, D., Unger, N., Yao, M., and Zhang, S.: Climate simulations for 1880-2003 with GISS modelE, 29, 661–696, https://doi.org/10.1007/s00382-007-0255-8, 2007.

Harper, A. B., Williams, K. E., McGuire, P. C., Duran Rojas, M. C., Hemming, D., Verhoef, A., Huntingford, C., Rowland, L., Marthews, T., Breder Eller, C., Mathison, C., Nobrega, R. L. B., Gedney, N., Vidale, P. L., Otu-Larbi, F., Pandey, D., Garrigues, S., Wright, A., Slevin, D., De Kauwe, M. G., Blyth, E., Ardö, J., Black, A., Bonal, D., Buchmann, N., Burban, B., Fuchs, K., de Grandcourt, A., Mammarella, I., Merbold, L., Montagnani, L., Nouvellon, Y., Restrepo-Coupe, N., and Wohlfahrt, G.: Improvement of modeling plant responses to low soil moisture in JULESvn4.9 and evaluation against flux tower measurements, 14, 3269–3294, https://doi.org/10.5194/gmd-14-3269-2021, 2021.

Harrison, S. P., Cramer, W., Franklin, O., Prentice, I. C., Wang, H., Brännström, Å., de Boer, H., Dieckmann, U., Joshi, J., Keenan, T. F., Lavergne, A., Manzoni, S., Mengoli, G., Morfopoulos, C., Peñuelas, J., Pietsch, S., Rebel, K. T., Ryu, Y., Smith, N. G., Stocker, B. D., and Wright, I. J.: Eco-evolutionary optimality as a means to improve vegetation and land-surface models, 231, 2125–2141, https://doi.org/10.1111/nph.17558, 2021.

Hengeveld, G. M., Gunia, K., Didion, M., Zudin, S., Clerkx, A. P. P. M., and Schelhaas, M. J.: Global 1-degree Maps of Forest Area, Carbon Stocks, and Biomass, 1950-2010, , https://doi.org/10.3334/ORNLDAAC/1296, 2015.

Hikosaka, K. and Anten, N. P. R.: An evolutionary game of leaf dynamics and its consequences for canopy structure, 26, 1024–1032, https://doi.org/10.1111/j.1365-2435.2012.02042.x, 2012.

Hourdin, F., Mauritsen, T., Gettelman, A., Golaz, J.-C., Balaji, V., Duan, Q., Folini, D., Ji, D., Klocke, D., Qian, Y., Rauser, F., Rio, C., Tomassini, L., Watanabe, M., and Williamson, D.: The Art and Science of Climate Model Tuning, 98, 589–602, https://doi.org/10.1175/BAMS-D-15-00135.1, 2017.

Huang, M., Piao, S., Sun, Y., Ciais, P., Cheng, L., Mao, J., Poulter, B., Shi, X., Zeng, Z., and Wang, Y.: Change in terrestrial ecosystem water-use efficiency over the last three decades, 21, 2366–2378, https://doi.org/10.1111/gcb.12873, 2015.

Huntzinger, D. N., Schwalm, C., Michalak, A. M., Schaefer, K., King, A. W., Wei, Y., Jacobson, A., Liu, S., Cook, R. B., Post, W. M., Berthier, G., Hayes, D., Huang, M., Ito, A., Lei, H., Lu, C., Mao, J., Peng, C. H., Peng, S., Poulter, B., Riccuito, D., Shi, X., Tian, H., Wang, W., Zeng, N., Zhao, F., and Zhu, Q.: The North American Carbon Program Multi-Scale Synthesis and Terrestrial Model Intercomparison Project – Part 1: Overview and experimental design, 6, 2121–2133, https://doi.org/10.5194/gmd-6-2121-2013, 2013.

Ito, G., Romanou, A., Kiang, N. Y., Faluvegi, G., Aleinov, I., Ruedy, R., Russell, G., Lerner, P., Kelley, M., and Lo, K.: Global Carbon Cycle and Climate Feedbacks in the NASA GISS ModelE2.1, 12, e2019MS002030, https://doi.org/10.1029/2019MS002030, 2020.

Jiang, L., Shi, Z., Xia, J., Liang, J., Lu, X., Wang, Y., and Luo, Y.: Transient Traceability Analysis of Land Carbon Storage Dynamics: Procedures and Its Application to Two Forest Ecosystems, 9, 2822–2835, https://doi.org/10.1002/2017MS001004, 2017.

Keenan, T. F., Hollinger, D. Y., Bohrer, G., Dragoni, D., Munger, J. W., Schmid, H. P., and Richardson, A. D.: Increase in forest water-use efficiency as atmospheric carbon dioxide concentrations rise, 499, 324–327, https://doi.org/10.1038/nature12291, 2013.

Kelley, M., Schmidt, G. A., Nazarenko, L. S., Bauer, S. E., Ruedy, R., Russell, G. L., Ackerman, A. S., Aleinov, I., Bauer, M., Bleck, R., Canuto, V., Cesana, G., Cheng, Y., Clune, T. L., Cook, B. I., Cruz, C. A., Del Genio, A. D., Elsaesser, G. S., Faluvegi, G., Kiang, N. Y., Kim, D., Lacis, A. A., Leboissetier, A., LeGrande, A. N., Lo, K. K., Marshall, J., Matthews, E. E., McDermid, S., Mezuman, K., Miller, R. L., Murray, L. T., Oinas, V., Orbe, C., García-Pando, C. P., Perlwitz, J. P., Puma, M. J., Rind, D., Romanou, A., Shindell, D. T., Sun, S., Tausnev, N., Tsigaridis, K., Tselioudis, G., Weng, E., Wu, J., and Yao, M.-S.: GISS-E2.1: Configurations and Climatology, Journal of Advances in Modeling Earth Systems, 12, e2019MS002025, https://doi.org/10.1029/2019MS002025, 2020.

Kim, Y., Moorcroft, P. R., Aleinov, I., Puma, M. J., and Kiang, N. Y.: Variability of phenology and fluxes of water and carbon with observed and simulated soil moisture in the Ent Terrestrial Biosphere Model (Ent TBM version 1.0.1.0.0), 8, 3837–3865, https://doi.org/10.5194/gmd-8-3837-2015, 2015.

Kyker-Snowman, E., Lombardozzi, D. L., Bonan, G. B., Cheng, S. J., Dukes, J. S., Frey, S. D., Jacobs, E. M., McNellis, R., Rady, J. M., Smith, N. G., Thomas, R. Q., Wieder, W. R., and Grandy, A. S.: Increasing the spatial and temporal impact of ecological research: A roadmap for integrating a novel terrestrial process into an Earth system model, 28, 665–684, https://doi.org/10.1111/gcb.15894, 2022.

Litton, C. M., Raich, J. W., and Ryan, M. G.: Carbon allocation in forest ecosystems, Global Change Biol, 13, 2089–2109, https://doi.org/10.1111/j.1365-2486.2007.01420.x, 2007.

Liu, H., Gleason, S. M., Hao, G., Hua, L., He, P., Goldstein, G., and Ye, Q.: Hydraulic traits are coordinated with maximum plant height at the global scale, 5, eaav1332, https://doi.org/10.1126/sciadv.aav1332, 2019.

Lloret, F., Escudero, A., Iriondo, J. M., Martínez-Vilalta, J., and Valladares, F.: Extreme climatic events and vegetation: the role of stabilizing processes, 18, 797–805, https://doi.org/10.1111/j.1365-2486.2011.02624.x, 2012.

Lu, R., Qiao, Y., Wang, J., Zhu, C., Cui, E., Xu, X., He, Y., Zhao, Z., Du, Y., Yan, L., Shen, G., Yang, Q., Wang, X., and Xia, J.: The U-shaped pattern of size-dependent mortality and its correlated factors in a subtropical monsoon evergreen forest, 109, 2421–2433, https://doi.org/10.1111/1365-2745.13652, 2021.

Luo, Y.: Terrestrial carbon-cycle feedback to climate warming, 38, 683–712, https://doi.org/10.1146/annurev.ecolsys.38.091206.095808, 2007.

Luo, Y. and Schuur, E. A. G.: Model parameterization to represent processes at unresolved scales and changing properties of evolving systems, 26, 1109–1117, https://doi.org/10.1111/gcb.14939, 2020.

Luo, Y. and Weng, E.: Dynamic disequilibrium of the terrestrial carbon cycle under global change, 26, 96–104, https://doi.org/10.1016/j.tree.2010.11.003, 2011.

Luo, Y., Weng, E., Wu, X., Gao, C., Zhou, X., and Zhang, L.: Parameter identifiability, constraint, and equifinality in data assimilation with ecosystem models, 19, 571–574, https://doi.org/10.1890/08-0561.1, 2009.

Luo, Y. Q., Randerson, J. T., Abramowitz, G., Bacour, C., Blyth, E., Carvalhais, N., Ciais, P., Dalmonech, D., Fisher, J. B., Fisher, R., Friedlingstein, P., Hibbard, K., Hoffman, F., Huntzinger, D., Jones, C. D., Koven, C., Lawrence, D., Li, D. J., Mahecha, M., Niu, S. L., Norby, R., Piao, S. L., Qi, X., Peylin, P., Prentice, I. C., Riley, W., Reichstein, M., Schwalm, C., Wang, Y. P., Xia, J. Y., Zaehle, S., and Zhou, X. H.: A framework for benchmarking land models, 9, 3857–3874, https://doi.org/10.5194/bg-9-3857-2012, 2012.

MacBean, N., Peylin, P., Chevallier, F., Scholze, M., and Schuermann, G.: Consistent assimilation of multiple data streams in a carbon cycle data assimilation system, 9, 3569–3588, https://doi.org/10.5194/gmd-9-3569-2016, 2016.

Manzoni, S., Trofymow, J. A., Jackson, R. B., and Porporato, A.: Stoichiometric controls on carbon, nitrogen, and phosphorus dynamics in decomposing litter, 80, 89–106, 2010.

Manzoni, S., Vico, G., Thompson, S., Beyer, F., and Weih, M.: Contrasting leaf phenological strategies optimize carbon gain under droughts of different duration, Advances in Water Resources, 84, 37–51, https://doi.org/10.1016/j.advwatres.2015.08.001, 2015.

McDowell, N. G.: Mechanisms Linking Drought, Hydraulics, Carbon Metabolism, and Vegetation Mortality, 155, 1051–1059, https://doi.org/10.1104/pp.110.170704, 2011.

McDowell, N. G., Allen, C. D., Anderson-Teixeira, K., Aukema, B. H., Bond-Lamberty, B., Chini, L., Clark, J. S., Dietze, M., Grossiord, C., Hanbury-Brown, A., Hurtt, G. C., Jackson, R. B., Johnson, D. J., Kueppers, L., Lichstein, J. W., Ogle, K., Poulter, B., Pugh, T. A. M., Seidl, R., Turner, M. G., Uriarte, M., Walker, A. P., and Xu, C.: Pervasive shifts in forest dynamics in a changing world, 368, https://doi.org/10.1126/science.aaz9463, 2020.

McNickle, G. G., Gonzalez-Meler, M. A., Lynch, D. J., Baltzer, J. L., and Brown, J. S.: The world's biomes and primary production as a triple tragedy of the commons foraging game played among plants, 283, 20161993, https://doi.org/10.1098/rspb.2016.1993, 2016.

Meir, P., Cox, P., and Grace, J.: The influence of terrestrial ecosystems on climate, Trends in Ecology & Evolution, 21, 254–260, https://doi.org/10.1016/j.tree.2006.03.005, 2006.

van der Molen, M. K., Dolman, A. J., Ciais, P., Eglin, T., Gobron, N., Law, B. E., Meir, P., Peters, W., Phillips, O. L., Reichstein, M., Chen, T., Dekker, S. C., Doubková, M., Friedl, M. A., Jung, M., van den Hurk, B. J. J. M., de Jeu, R. A. M., Kruijt, B., Ohta, T., Rebel, K. T., Plummer, S., Seneviratne, S. I., Sitch, S., Teuling, A. J., van der Werf, G. R., and Wang, G.: Drought and ecosystem carbon cycling, Agricultural and Forest Meteorology, 151, 765–773, https://doi.org/10.1016/j.agrformet.2011.01.018, 2011.

Montané, F., Fox, A. M., Arellano, A. F., MacBean, N., Alexander, M. R., Dye, A., Bishop, D. A., Trouet, V., Babst, F., Hessl, A. E., Pederson, N., Blanken, P. D., Bohrer, G., Gough, C. M., Litvak, M. E., Novick, K. A., Phillips, R. P., Wood, J. D., and Moore, D. J. P.: Evaluating the effect of alternative carbon allocation schemes in a land surface model (CLM4.5) on carbon fluxes, pools, and turnover in temperate forests, 10, 3499–3517, https://doi.org/10.5194/gmd-10-3499-2017, 2017.

Niinemets, Ü. and Anten, N. P. R.: Packing the Photosynthetic Machinery: From Leaf to Canopy, in: Photosynthesis in silico: Understanding Complexity from Molecules to Ecosystems, edited by: Laisk, A., Nedbal, L., and Govindjee, Springer Netherlands, Dordrecht, 363–399, https://doi.org/10.1007/978-1-4020-9237-4_16, 2009.

Niinemets, Ü., Keenan, T. F., and Hallik, L.: A worldwide analysis of within-canopy variations in leaf structural, chemical and physiological traits across plant functional types, 205, 973–993, https://doi.org/10.1111/nph.13096, 2015.

Niklas, K.: Plant Height and the Properties of Some Herbaceous Stems, 75, 133–142, https://doi.org/10.1006/anbo.1995.1004, 1995.

Nobre, C. A., Sellers, P. J., and Shukla, J.: Amazonian Deforestation and Regional Climate Change, J. Climate, 4, 957–988, https://doi.org/10.1175/1520-0442(1991)004<0957:ADARCC>2.0.CO;2, 1991.

Oliveira, R. S., Eller, C. B., Barros, F. de V., Hirota, M., Brum, M., and Bittencourt, P.: Linking plant hydraulics and the fast–slow continuum to understand resilience to drought in tropical ecosystems, 230, 904–923, https://doi.org/10.1111/nph.17266, 2021.

Osnas, J. L. D., Lichstein, J. W., Reich, P. B., and Pacala, S. W.: Global Leaf Trait Relationships: Mass, Area, and the Leaf Economics Spectrum, 340, 741–744, https://doi.org/10.1126/science.1231574, 2013.

Pan, Y., Birdsey, R. A., Phillips, O. L., and Jackson, R. B.: The Structure, Distribution, and Biomass of the World's Forests, 44, 593–622, https://doi.org/10.1146/annurev-ecolsys-110512-135914, 2013.

Parton, W., Schimel, D., Cole, C., and Ojima, D.: Analysis of factors controlling soil organic matter levels in Great Plains grasslands, 51, 1173–1179, https://doi.org/10.2136/sssaj1987.03615995005100050015x, 1987.

Parton, W. J., Stewart, J., and Cole, C.: DYNAMICS OF C, N, P AND S IN GRASSLAND SOILS - A MODEL, 5, 109–131, https://doi.org/10.1007/BF02180320, 1988.

Pavlick, R., Drewry, D. T., Bohn, K., Reu, B., and Kleidon, A.: The Jena Diversity-Dynamic Global Vegetation Model (JeDi-DGVM): a diverse approach to representing terrestrial biogeography and biogeochemistry based on plant functional trade-offs, 10, 4137–4177, https://doi.org/10.5194/bg-10-4137-2013, 2013.

Pielke, R. A., Sr, ., Avissar, RonI., Raupach, M., Dolman, A. J., Zeng, X., and Denning, A. S.: Interactions between the atmosphere and terrestrial ecosystems: influence on weather and climate, 4, 461–475, https://doi.org/10.1046/j.1365-2486.1998.t01-1-00176.x, 1998.

Potter, C., Klooster, S., Myneni, R., Genovese, V., Tan, P., and Kumar, V.: Continental-scale comparisons of terrestrial carbon sinks estimated from satellite data and ecosystem modeling 1982-1998, 39, 201–213, https://doi.org/10.1016/j.gloplacha.2003.07.001, 2003.

Potter, C. S., Randerson, J. T., Field, C. B., Matson, P. A., Vitousek, P. M., Mooney, H. A., and Klooster, S. A.: Terrestrial ecosystem production: A process model based on global satellite and surface data, 7, 811–841, https://doi.org/10.1029/93GB02725, 1993.

Powell, T. L., Galbraith, D. R., Christoffersen, B. O., Harper, A., Imbuzeiro, H. M. A., Rowland, L., Almeida, S., Brando, P. M., da Costa, A. C. L., Costa, M. H., Levine, N. M., Malhi, Y.,

Saleska, S. R., Sotta, E., Williams, M., Meir, P., and Moorcroft, P. R.: Confronting model predictions of carbon fluxes with measurements of Amazon forests subjected to experimental drought, 200, 350–365, https://doi.org/10.1111/nph.12390, 2013.

Prentice, I. C., Cramer, W., Harrison, S. P., LEEMANS, R., Monserud, R. A., and Solomon, A. M.: A global biome model based on plant physiology and dominance, soil properties and climate, 19, 117–134, https://doi.org/10.2307/2845499, 1992.

Prentice, I. C., Bondeau, A., Cramer, W., Harrison, S. P., Hickler, T., Lucht, W., Sitch, S., Smith, B., and Sykes, M. T.: Dynamic Global Vegetation Modeling: Quantifying Terrestrial Ecosystem Responses to Large-Scale Environmental Change, in: Terrestrial Ecosystems in a Changing World, edited by: Canadell, J. G., Pataki, D. E., and Pitelka, L. F., Springer Berlin Heidelberg, Berlin, Heidelberg, 175–192, https://doi.org/10.1007/978-3-540-32730-1_15, 2007.

Prentice, I. C., Dong, N., Gleason, S. M., Maire, V., and Wright, I. J.: Balancing the costs of carbon gain and water transport: testing a new theoretical framework for plant functional ecology, 17, 82–91, https://doi.org/10.1111/ele.12211, 2014.

Purves, D. and Pacala, S.: Predictive models of forest dynamics, 320, 1452–1453, https://doi.org/10.1126/science.1155359, 2008.

Purves, D. W., Lichstein, J. W., Strigul, N., and Pacala, S. W.: Predicting and understanding forest dynamics using a simple tractable model, 105, 17018–17022, https://doi.org/10.1073/pnas.0807754105, 2008.

Randerson, J., Thompson, M., Conway, T., Fung, I., and Field, C.: The contribution of terrestrial sources and sinks to trends in the seasonal cycle of atmospheric carbon dioxide, 11, 535–560, https://doi.org/10.1029/97GB02268, 1997.

Reich, P. B.: The world-wide 'fast–slow' plant economics spectrum: a traits manifesto, 102, 275–301, https://doi.org/10.1111/1365-2745.12211, 2014.

Reyer, C. P. O., Leuzinger, S., Rammig, A., Wolf, A., Bartholomeus, R. P., Bonfante, A., de Lorenzi, F., Dury, M., Gloning, P., Abou Jaoudé, R., Klein, T., Kuster, T. M., Martins, M., Niedrist, G., Riccardi, M., Wohlfahrt, G., de Angelis, P., de Dato, G., François, L., Menzel, A., and Pereira, M.: A plant's perspective of extremes: terrestrial plant responses to changing climatic variability, 19, 75–89, https://doi.org/10.1111/gcb.12023, 2013.

Rodriguez-Iturbe, I., Porporato, A., Ridolfi, L., Isham, V., and Coxi, D. R.: Probabilistic modelling of water balance at a point: the role of climate, soil and vegetation, 455, 3789–3805, https://doi.org/10.1098/rspa.1999.0477, 1999.

Rosenzweig, C. and Abramopoulos, F.: Land-Surface Model Development for the GISS GCM, 10, 2040–2054, https://doi.org/10.1175/1520-0442(1997)010<2040:LSMDFT>2.0.CO;2, 1997.

Scheiter, S., Langan, L., and Higgins, S. I.: Next-generation dynamic global vegetation models: learning from community ecology, 198, 957–969, https://doi.org/10.1111/nph.12210, 2013.

Schmidt, G. A., Kelley, M., Nazarenko, L., Ruedy, R., Russell, G. L., Aleinov, I., Bauer, M., Bauer, S. E., Bhat, M. K., Bleck, R., Canuto, V., Chen, Y.-H., Cheng, Y., Clune, T. L., Del Genio, A., de Fainchtein, R., Faluvegi, G., Hansen, J. E., Healy, R. J., Kiang, N. Y., Koch,

D., Lacis, A. A., LeGrande, A. N., Lerner, J., Lo, K. K., Matthews, E. E., Menon, S., Miller, R. L., Oinas, V., Oloso, A. O., Perlwitz, J. P., Puma, M. J., Putman, W. M., Rind, D., Romanou, A., Sato, M., Shindell, D. T., Sun, S., Syed, R. A., Tausnev, N., Tsigaridis, K., Unger, N., Voulgarakis, A., Yao, M.-S., and Zhang, J.: Configuration and assessment of the GISS ModelE2 contributions to the CMIP5 archive, 6, 141–184, https://doi.org/10.1002/2013MS000265, 2014.

Sellers, P. J.: Modeling the Exchanges of Energy, Water, and Carbon Between Continents and the Atmosphere, 275, 502–509, https://doi.org/10.1126/science.275.5299.502, 1997.

Sierra, C. A., Ceballos-Núñez, V., Metzler, H., and Müller, M.: Representing and Understanding the Carbon Cycle Using the Theory of Compartmental Dynamical Systems, 10, 1729–1734, https://doi.org/10.1029/2018MS001360, 2018.

Simard, M., Pinto, N., Fisher, J. B., and Baccini, A.: Mapping forest canopy height globally with spaceborne lidar, 116, https://doi.org/10.1029/2011JG001708, 2011.

Singh, A. K., Dhanapal, S., and Yadav, B. S.: The dynamic responses of plant physiology and metabolism during environmental stress progression, Mol Biol Rep, 47, 1459–1470, https://doi.org/10.1007/s11033-019-05198-4, 2020.

Sitch, S., Smith, B., Prentice, I. C., Arneth, A., Bondeau, A., Cramer, W., Kaplan, J. O., Levis, S., Lucht, W., Sykes, M. T., Thonicke, K., and Venevsky, S.: Evaluation of ecosystem dynamics, plant geography and terrestrial carbon cycling in the LPJ dynamic global vegetation model, 9, 161–185, https://doi.org/10.1046/j.1365-2486.2003.00569.x, 2003.

Sitch, S., Friedlingstein, P., Gruber, N., Jones, S. D., Murray-Tortarolo, G., Ahlström, A., Doney, S. C., Graven, H., Heinze, C., Huntingford, C., Levis, S., Levy, P. E., Lomas, M., Poulter, B., Viovy, N., Zaehle, S., Zeng, N., Arneth, A., Bonan, G., Bopp, L., Canadell, J. G., Chevallier, F., Ciais, P., Ellis, R., Gloor, M., Peylin, P., Piao, S. L., Le Quéré, C., Smith, B., Zhu, Z., and Myneni, R.: Recent trends and drivers of regional sources and sinks of carbon dioxide, Biogeosciences, 12, 653–679, https://doi.org/10.5194/bg-12-653-2015, 2015.

Strigul, N., Pristinski, D., Purves, D., Dushoff, J., and Pacala, S.: Scaling from trees to forests: tractable macroscopic equations for forest dynamics, 78, 523–545, https://doi.org/10.1890/08-0082.1, 2008.

Swenson, N. G. and Enquist, B. J.: Ecological and evolutionary determinants of a key plant functional trait: wood density and its community-wide variation across latitude and elevation, 94, 451–459, https://doi.org/10.3732/ajb.94.3.451, 2007.

Tifafi, M., Guenet, B., and Hatté, C.: Large Differences in Global and Regional Total Soil Carbon Stock Estimates Based on SoilGrids, HWSD, and NCSCD: Intercomparison and Evaluation Based on Field Data From USA, England, Wales, and France, 32, 42–56, https://doi.org/10.1002/2017GB005678, 2018.

Tilman, D.: Plant strategies and the dynamics and structure of plant communities, Princeton University Press, Princeton, N.J, 360 pp., 1988.

Verryckt, L. T., Vicca, S., Van Langenhove, L., Stahl, C., Asensio, D., Urbina, I., Ogaya, R., Llusià, J., Grau, O., Peguero, G., Gargallo-Garriga, A., Courtois, E. A., Margalef, O., Portillo-Estrada, M., Ciais, P., Obersteiner, M., Fuchslueger, L., Lugli, L. F., Fernandez-

Garberí, P.-R., Vallicrosa, H., Verlinden, M., Ranits, C., Vermeir, P., Coste, S., Verbruggen, E., Bréchet, L., Sardans, J., Chave, J., Peñuelas, J., and Janssens, I. A.: Vertical profiles of leaf photosynthesis and leaf traits and soil nutrients in two tropical rainforests in French Guiana before and after a 3-year nitrogen and phosphorus addition experiment, 14, 5–18, https://doi.org/10.5194/essd-14-5-2022, 2022.

Volaire, F.: A unified framework of plant adaptive strategies to drought: Crossing scales and disciplines, 24, 2929–2938, https://doi.org/10.1111/gcb.14062, 2018.

Wang, H., Prentice, I. C., Keenan, T. F., Davis, T. W., Wright, I. J., Cornwell, W. K., Evans, B. J., and Peng, C.: Towards a universal model for carbon dioxide uptake by plants, 3, 734–741, https://doi.org/10.1038/s41477-017-0006-8, 2017.

Wang, Y.-P. and Goll, D. S.: Modelling of land nutrient cycles: recent progress and future development, Fac Rev, 10, 53, https://doi.org/10.12703/r/10-53, 2021.

Wang, Y.-P., Trudinger, C. M., and Enting, I. G.: A review of applications of model–data fusion to studies of terrestrial carbon fluxes at different scales, 149, 1829–1842, https://doi.org/10.1016/j.agrformet.2009.07.009, 2009.

Wei, N., Xia, J., Zhou, J., Jiang, L., Cui, E., Ping, J., and Luo, Y.: Evolution of Uncertainty in Terrestrial Carbon Storage in Earth System Models from CMIP5 to CMIP6, 1, 1–33, https://doi.org/10.1175/JCLI-D-21-0763.1, 2022.

Weng, E. and Luo, Y.: Relative information contributions of model vs. data to short- and long-term forecasts of forest carbon dynamics, 21, 1490–1505, 2011.

Weng, E., Luo, Y., Gao, C., and Oren, R.: Uncertainty analysis of forest carbon sink forecast with varying measurement errors: a data assimilation approach, 4, 178–191, https://doi.org/10.1093/jpe/rtr018, 2011.

Weng, E., Farrior, C. E., Dybzinski, R., and Pacala, S. W.: Predicting vegetation type through physiological and environmental interactions with leaf traits: evergreen and deciduous forests in an earth system modeling framework, 23, 2482–2498, https://doi.org/10.1111/gcb.13542, 2017.

Weng, E., Dybzinski, R., Farrior, C. E., and Pacala, S. W.: Competition alters predicted forest carbon cycle responses to nitrogen availability and elevated CO2: simulations using an explicitly competitive, game-theoretic vegetation demographic model, 16, 4577–4599, https://doi.org/10.5194/bg-16-4577-2019, 2019.

Weng, E. S., Malyshev, S., Lichstein, J. W., Farrior, C. E., Dybzinski, R., Zhang, T., Shevliakova, E., and Pacala, S. W.: Scaling from individual trees to forests in an Earth system modeling framework using a mathematically tractable model of height-structured competition, 12, 2655–2694, https://doi.org/10.5194/bg-12-2655-2015, 2015.

Wieder, W. R.: Regridded Harmonized World Soil Database v1.2, , https://doi.org/10.3334/ORNLDAAC/1247, 2014.

Wieder, W. R., Grandy, A. S., Kallenbach, C. M., and Bonan, G. B.: Integrating microbial physiology and physio-chemical principles in soils with the MIcrobial-MIneral Carbon Stabilization (MIMICS) model, 11, 3899–3917, https://doi.org/10.5194/bg-11-3899-2014, 2014.

Williams, M., Richardson, A. D., Reichstein, M., Stoy, P. C., Peylin, P., Verbeeck, H., Carvalhais, N., Jung, M., Hollinger, D. Y., Kattge, J., Leuning, R., Luo, Y., Tomelleri, E., Trudinger, C. M., and Wang, Y.-P.: Improving land surface models with FLUXNET data, Biogeosciences, 6, 1341–1359, https://doi.org/10.5194/bg-6-1341-2009, 2009.

Woodward, F. I., Lomas, M. R., and Betts, R. A.: Vegetation-climate feedbacks in a greenhouse world, Phil. Trans. R. Soc. Lond. B, 353, 29–39, https://doi.org/10.1098/rstb.1998.0188, 1998.

Xia, J., Luo, Y., Wang, Y.-P., and Hararuk, O.: Traceable components of terrestrial carbon storage capacity in biogeochemical models, 19, 2104–2116, https://doi.org/10.1111/gcb.12172, 2013.

Xia, J., Yuan, W., Wang, Y.-P., and Zhang, Q.: Adaptive Carbon Allocation by Plants Enhances the Terrestrial Carbon Sink, Sci Rep, 7, 3341, https://doi.org/10.1038/s41598-017-03574-3, 2017.

Xia, J., Yuan, W., Lienert, S., Joos, F., Ciais, P., Viovy, N., Wang, Y., Wang, X., Zhang, H., Chen, Y., and Tian, X.: Global Patterns in Net Primary Production Allocation Regulated by Environmental Conditions and Forest Stand Age: A Model-Data Comparison, 124, 2039–2059, https://doi.org/10.1029/2018JG004777, 2019.

Xu, T., White, L., Hui, D., and Luo, Y.: Probabilistic inversion of a terrestrial ecosystem model: Analysis of uncertainty in parameter estimation and model prediction, 20, GB2007, https://doi.org/10.1029/2005GB002468, 2006.

Yuan, W., Luo, Y., Liang, S., Yu, G., Niu, S., Stoy, P., Chen, J., Desai, A. R., Lindroth, A., Gough, C. M., Ceulemans, R., Arain, A., Bernhofer, C., Cook, B., Cook, D. R., Dragoni, D., Gielen, B., Janssens, I. A., Longdoz, B., Liu, H., Lund, M., Matteucci, G., Moors, E., Scott, R. L., Seufert, G., and Varner, R.: Thermal adaptation of net ecosystem exchange, 8, 1453–1463, https://doi.org/10.5194/bg-8-1453-2011, 2011.

Zeng, Z., Piao, S., Li, L. Z. X., Zhou, L., Ciais, P., Wang, T., Li, Y., Lian, X., Wood, E. F., Friedlingstein, P., Mao, J., Estes, L. D., Myneni, R. B., Peng, S., Shi, X., Seneviratne, S. I., and Wang, Y.: Climate mitigation from vegetation biophysical feedbacks during the past three decades, 7, 432–436, https://doi.org/10.1038/nclimate3299, 2017.

Zhou, G., Houlton, B. Z., Wang, W., Huang, W., Xiao, Y., Zhang, Q., Liu, S., Cao, M., Wang, X., Wang, S., Zhang, Y., Yan, J., Liu, J., Tang, X., and Zhang, D.: Substantial reorganization of China's tropical and subtropical forests: based on the permanent plots, 20, 240–250, https://doi.org/10.1111/gcb.12385, 2014.

Zhou, J., Xia, J., Wei, N., Liu, Y., Bian, C., Bai, Y., and Luo, Y.: A traceability analysis system for model evaluation on land carbon dynamics: design and applications, Ecol Process, 10, 12, https://doi.org/10.1186/s13717-021-00281-w, 2021.

Zuleta, D., Arellano, G., Muller-Landau, H. C., McMahon, S. M., Aguilar, S., Bunyavejchewin, S., Cárdenas, D., Chang-Yang, C.-H., Duque, A., Mitre, D., Nasardin, M., Pérez, R., Sun, I.-F., Yao, T. L., and Davies, S. J.: Individual tree damage dominates mortality risk factors across six tropical forests, 233, 705–721, https://doi.org/10.1111/nph.17832, 2022.